AN INVESTIGATION OF THE EFFECTS OF A LOSSY EARTH ON ANTENNA PATTERNS AT VHF

Edward H. Newman

Ohio State University

Prepared for:

Harry Diamond Laboratories

December 1972

3281-1

AN INVESTIGATION OF THE EFFECTS OF A LOSSY EARTH ON ANTENNA PATTERNS AT VHF

by

Edward H. Newman

Prepared by:

The Ohio State University

ElectroScience Laboratory

Department of Electrical Engineering
Columbus, Ohio 43212

Under Contract Number
DAAG-39-72-C-0041

December 1972

United States Army Materiel Command
HARRY DIAMOND LABORATORIES
Washington, D.C. 20438

NOTICES

When Government drawings, specifications, or other data are used for any purpose other than in connection with a definitely related Government procurement operation, the United States Government thereby incurs no responsibility nor any obligation whatsoever, and the fact that the Government may have formulated, furnished, or in any way supplied the said drawings, specifications, or other data, is not to be regarded by implication or otherwise as in any manner licensing the holder or any other person or corporation, or conveying any rights or permission to manufacture, use, or sell any patented invention that may in any way be related thereto.

The findings in this report are not to be construed as an official Department of the Army position unless so designated by other authorized documents.

Citation of manufacturers' or trade names does not constitute an official indorsement or approval of the use thereof.

Destroy this report when it is no longer needed. Do not return it to the originator.

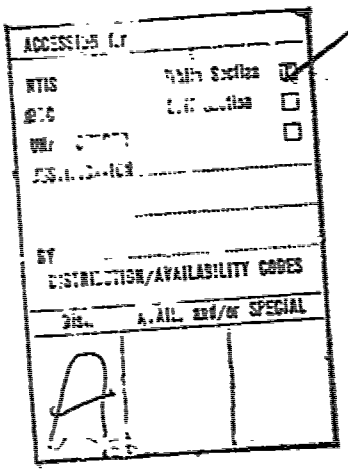

AMCMS CODE 5917-22-70409
HDL PROJ 117215

3281-1

AN INVESTIGATION OF THE EFFECTS OF A LOSSY EARTH ON ANTENNA PATTERNS AT VHF

by
Edward H. Newman

Prepared by:

ELECTROSCIENCE LABORATORY
OHIO STATE UNIVERSITY
COLUMBUS, OHIO

Under Contract Number
DAAG-39-72-C-0041

December 1972

United States Army Materiel Command
HARRY DIAMOND LABORATORIES
Washington, D.C. 20438

UNCLASSIFIED
Security Classification

DOCUMENT CONTROL DATA - R & D

Security classification of title, body of abstract and indexing annotation must be entered when the overall report is classified.

1 ORIGINATING ACTIVITY (Corporate author) The Ohio State University ElectroScience Laboratory, Department of Electrical Engineering, Columbus Ohio 43212	2a. REPORT SECURITY CLASSIFICATION Unclassified 2b. GROUP

3 REPORT TITLE

AN INVESTIGATION OF THE EFFECTS OF A LOSSY EARTH ON ANTENNA PATTERNS AT VHF

4 DESCRIPTIVE NOTES (Type of report and inclusive dates)

Technical Report

5 AUTHOR(S) (First name, middle initial, last name)

Newman, Edward H.

6 REPORT DATE	7a. TOTAL NO OF PAGES	7b. NO OF REFS
December 1972	68	16

8a. CONTRACT OR GRANT NO	9a. ORIGINATOR'S REPORT NUMBER(S)
DAAG-39-72-C-0041 b. PROJECT NO c. AMCMS CODE 5917.22.70409 d. HDL PROJ 117215	HDL 3281-1 9b. OTHER REPORT NO(S) (Any other numbers that may be assigned this report)

10 DISTRIBUTION STATEMENT

Approved for public release; distribution unlimited

11 SUPPLEMENTARY NOTES	12. SPONSORING MILITARY ACTIVITY
	Harry Diamond Labs Electronics Command

13 ABSTRACT

The objective of this report is to theoretically investigate the potential of several low profile antennas for use at or near ground level locations, as compared with a quarter wavelength monopole. Of specific interest is the radiated field intensity at low elevation angles produced by VHF multiturn loop antennas having various orientations with respect to a flat lossy earth.

To accomplish the objective stated above, we start with Norton's classical expressions for an antenna over a flat lossy earth and obtain a qualitative indication as to how the presence of a lossy earth affects the far-field power pattern of an antenna in air located above the lossy earth. This includes a description of the fields in terms of space waves and surface waves, and a parameter study to determine the effects on the far-field pattern of varying the pattern radius, the ground constants, and the antenna height above the earth. Next a computationally straightforward method for determining the far-field pattern of an antenna located near a lossy earth is described. This method is then used to calculate the far-field power patterns of a few electrically small multiturn loop antennas.

DD FORM 1 NOV 65 1473

UNCLASSIFIED
Security Classification

14 KEY WORDS	LINK A		LINK B		LINK C	
	ROLE	WT	ROLE	WT	ROLE	WT
Multiturn loop antennas Electrically small antennas Lossy earth Propagation						

ACKNOWLEDGMENTS

The author wishes to acknowledge the encouragement and advice of Professor C. H. Walter and P. Bohley. Special recognition is deserved by Professors G. A. Thiele and C. A. Levis for many helpful discussions and their critical reading of this manuscript, and also by Dr. P. K. Agrawal for aiding in the calculations.

ABSTRACT

The objective of this report is to theoretically investigate the potential of several low profile antennas for use at or near ground level locations, as compared with a quarter wavelength monopole. Of specific interest is the radiated field intensity at low elevation angles produced by VHF multiturn loop antennas having various orientations with respect to a flat lossy earth.

To accomplish the objective stated above, we start with Norton's classical expressions for an antenna over a flat lossy earth and obtain a qualitative indication as to how the presence of a lossy earth affects the far-field power pattern of an antenna in air located above the lossy earth. This includes a description of the fields in terms of space waves and surface waves, and a parameter study to determine the effects on the far-field pattern of varying the pattern radius, the ground constants, and the antenna height above the earth. Next a computationally straightforward method for determining the far-field pattern of an antenna located near a lossy earth is described. This method is then used to calculate the far-field power patterns of a few electrically small multiturn loop antennas.

TABLE OF CONTENTS

AN INVESTIGATION OF THE EFFECTS OF A LOSSY EARTH ON ANTENNA PATTERNS AT VHF

I. INTRODUCTION

The objective of this report is to theoretically investigate the potential of several low profile antennas for use at or near ground level locations such that the low angle radiation can be compared with that of a quarter wavelength monopole having four quarter wavelengths radial arms. Since the monopole is not necessarily vertical with respect to the earth, we are interested in pattern results for various tilt angles of both the monopole and the low profile antennas under investigation.

The principle low profile antenna of interest is the multiturn loop antenna on a small ground plane tilted at various angles with respect to the lossy earth. Thus, there is a need to develope a method for calculating the far-field pattern of an arbitrarily shaped antenna having an arbitrary orientation with respect to the earth. Therefore, a secondary objective of this report is to describe a method for doing this.

In Section II a computationally straightforward method for performing the calculations described above is presented. The method is based on the assumption that the antenna current is not affected by the lossy ground and gives accurate radiation patterns for certain antennas over a flat lossy earth void of protruding vegetation, buildings, etc. In Section II, then, are presented the field equations used in determining the antenna patterns. The equations are interpreted in terms of space waves and surface waves

In Section III a parameter study is made using the theoretical expression of Section II to determine qualitatively the effects on an antenna's far-field pattern of the distance from the antenna to the observation point, the antenna geometry, and the conductivity and permittivity of the ground.

In Section IV we show how a continuous current distribution can be expressed in terms of a finite number of infinitesimal sources, and in Section V the results of Sections II and IV are used to calculate the far-field power patterns of four antennas.

Appendix I contains descriptions and listings of computer programs used, and Appendix II compares patterns calculated by the methods of this report with those found elsewhere in the literature.

II. THEORY

In this section we wish to describe a computationally straight forward method for determining the radiated fields of an antenna located over an infinite flat ground plane of arbitrary permittivity, and conductivity. A number of approximations are made and these are described along with their resulting limitations in the text to follow. The method is best applicable to electrically small antennas which are at least partially shielded from the lossy earth by a small perfectly conducting ground plane or by a cavity, and yields the radiated fields to within a few wavelengths of the antenna. Electrically large antennas can be treated through the use of increased computer time.

The basic approximation in this method is that the antenna current with the antenna located in free space be identical to the current with the antenna located over a finitely conducting flat earth. Rigorously this is clearly not the case. However, it is a reasonable approximation for an antenna which is shielded from the finitely conducting earth as is the case for an antenna in a cavity or over a small ground plane, and it is these configurations that we will consider. A typical configuration is shown in Fig. 1.

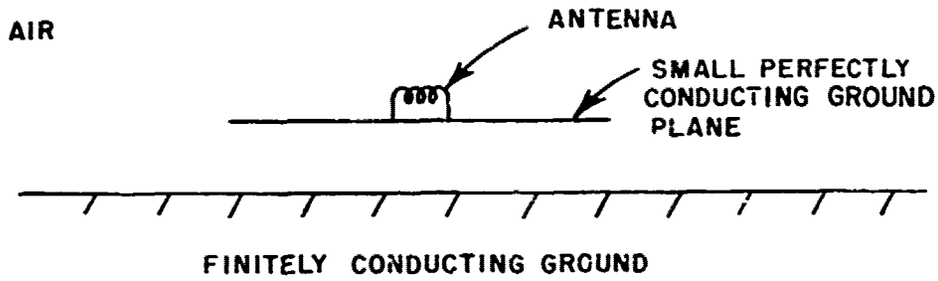

Fig. 1. Antenna shielded from ground by perfectly conducting ground plane.

Since small changes in a current distribution cause even smaller changes in the far-field pattern, our approximation is most applicable to determining far-field patterns.

The problem of determining the far-field pattern of an antenna must begin with a determination of the currents on the antenna. When the antenna is in the presence of a conducting earth this can be done using the rigorous Sommerfeld-integral approach[1-3], or by some approximate technique, one of which is a reflection coefficient approximation described by E. K. Miller et al[4,5]. The reflection

coefficient approximation is a technique using the Fresnel plane-wave reflection coefficients to account for the influence of fields reflected from the interface upon the antenna current distribution, and is found to yield the input impedance generally to within 10% of the results obtained by the rigorous method but at about 1% of the computer cost. Our approach is more approximate than either of the above, but has the advantage that computer programs already exist to evaluate the currents on antennas located in free space[6-9]. As previously mentioned, it is most applicable when the antenna is somehow shielded from the earth. However, it would also apply to antennas sufficiently elevated from the earth.

Assume now that by some method a current distribution has been determined on an antenna or a wire-grid model of the antenna. To find the fields radiated by this arbitrary current distribution we must first find the fields radiated by an arbitrarily orientated infinitesimal electric current element located in air and near a plane earth of relative permittivity ε_r, conductivity σ expressed in electromagnetic units, and permeability μ_0 of free space. (Note one electromagnetic unit or emu equals 10^{-11} mho/meter). To do this we can use expressions given by Norton[10].

Figure 2 shows the coordinate system to be used We let the

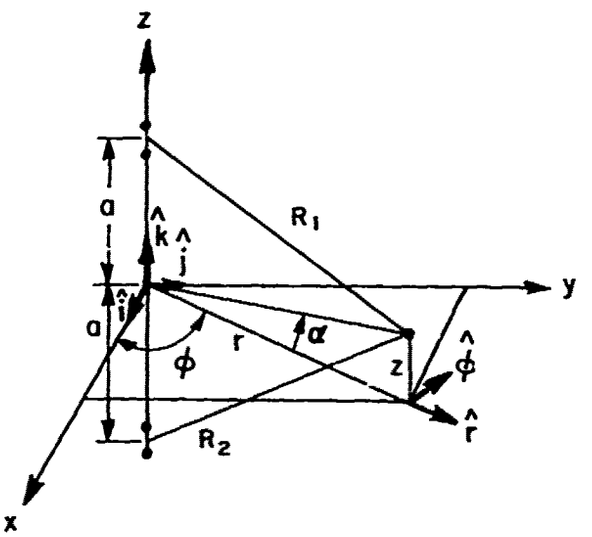

Fig. 2. Geometry for dipole radiation formulas.

origin of our coordinate system be at the surface of the earth under the current element and choose a right-handed set of unit vectors

$\hat{i}$, $\hat{j}$, and $\hat{k}$ in the direction of x, y, and z. The cylindrical coordinates r, ϕ, and z, and corresponding unit vectors $\hat{r}$, $\hat{\phi}$, and $\hat{k}$ are also shown. R_1, R_2, and a are defined in Fig. 2 and in addition

(1) $k = 2\pi/\lambda$, λ = free space wavelength

(2) $k_2^2 = k^2(\epsilon_r - j\chi)$

(3) $\chi = 1.8 \times 10^{18} \sigma_{emu}/f_{kc}$

(4) σ_{emu} = ground conductivity expressed in emu

(5) f_{kc} = frequency in kilocycles per second

(6) $R^2 = x^2+y^2+z^2$

(7) $u = k/k_2$.

Norton found simplified and computationally useful expressions for $\vec{E}$ and we will include some of them here. While Norton's expressions are valid in the upper half-space to within a few wavelengths of the source, the field components to follow are simplified for the far-field. By far-field in this report we mean $1/R \gg 1/R^2$. For a vertical electric current element, with $e^{j\omega t}$ time dependence surpressed, and located at z=a, x=y=0, as shown in Fig. 2,

$$(8) \quad E_z^v = -jk\left\{\cos^2\psi' \frac{e^{-jkR_1}}{R_1} + R_v \cos^2\psi' \frac{e^{-jkR_2}}{R_2} + (1-R_v)(1-u^2+u^4\cos^2\psi')\, F \frac{e^{-jkR_2}}{R_2}\right\}$$

where,

$$(9a) \quad R_v = (\sin\psi' - u\sqrt{1-u^2\cos^2\psi'})/(\sin\psi' + u\sqrt{1-u^2\cos^2\psi'})$$

$$(9b) \quad \sin\psi' = (z+a)/R_2$$

$$(9c) \quad F = [1-j\sqrt{\pi w}e^{-w}\ \mathrm{erfc}(j\sqrt{w})]$$

$$(9d) \quad w = 4p_1/(1-R_v)^2$$

$$(9e) \quad p_1 = p\, e^{-jb}$$

$$(9f) \quad p \cong \frac{-R_2 \cos b}{\chi\lambda}$$

(9g) $\tan b \cong (\epsilon_r + \cos^2\psi')/x$

(9h) $\sin\psi'' = (z-a)/R_1$.

In Eq. (8) the first two terms represent the direct or space wave radiation from the source and its image (located at z=-a, x=y=0) respectively, and both vary as 1/R. The last term represents the ground or surface wave radiation and varies as F/R. F is generally termed a ground wave attenuation function, and depends upon the earth's constants and upon the distance to the field point. p and b are generally termed the numerical distance and phase factor respectively for vertical dipoles. The remaining components for the vertical element are

$$(10)\qquad E_r^v = jk\cos\phi\left\{\sin\psi''\cos\psi''\,\frac{e^{-jkR_1}}{R_1} + R_v\sin\psi'\cos\psi'\,\frac{e^{-jkR_2}}{R_2}\right.$$
$$\left. - \cos\psi'(1-R_v)u\sqrt{1-u^2\cos^2\psi'}\;F\,\frac{e^{-jkR_2}}{R_2}\cdot\left(1 - \frac{u^2(1-u^2\cos^2\psi')}{2} + \frac{\sin^2\psi'}{2}\right)\right\}$$

$$(11)\qquad E_\phi^v = 0.$$

For a horizontal infinitesimal electric current element aligned with the x-axis

$$(12)\qquad E_z^h = -jk\cos\phi\left\{\sin\psi''\cos\psi''\,\frac{e^{-jkR_1}}{R_1} - R_v\sin\psi'\cos\psi'\,\frac{e^{-jkR_2}}{R_2}\right.$$
$$\left. + \cos\psi'(1-R_v)u\sqrt{1-u^2\cos^2\psi'}\;F\,\frac{e^{-jkR_2}}{R_2}\cdot\left(1 - \frac{u^2(1-u^2\cos^2\psi')}{2} + \frac{\sin^2\psi'}{2}\right)\right\}$$

$$(13)\qquad E_r^h = jk\cos\phi\left\{\sin^2\psi''\,\frac{e^{-jkR_1}}{R_1} - R_v\sin^2\psi'\,\frac{e^{-jkR_2}}{R_2}\right.$$
$$\left. + (1+R_h)\,G\,\frac{e^{-jkR_2}}{R_2} - \cos^2\psi' u^2(1-R_v)\,F\,\frac{e^{-jkR_2}}{R_2}\right\}$$

$$(14) \qquad E_\phi^h = -jk\sin\phi \left\{ \frac{e^{-jkR_1}}{R_1} - R_h \frac{e^{-jkR_2}}{R_2} + (1+R_h)\, G \frac{e^{-jkR_2}}{R_2} \right\}$$

where,

$$(15a) \qquad R_h = (\sqrt{1-u^2\cos^2\psi'} - u\sin\psi')/(\sqrt{1-u^2\cos^2\psi'} + u\sin\psi')$$

$$(15b) \qquad G = [1-j\sqrt{\pi v}\, e^{-v}\, \mathrm{erfc}(j\sqrt{v})]$$

$$(15c) \qquad v = 4q_1/(1+R_h)^2$$

$$(15d) \qquad q_1 = -q\, e^{jb'}$$

$$(15e) \qquad q \cong \frac{\pi\chi R_2}{\lambda\cos(b')}$$

$$(15f) \qquad \tan(b') \cong (\varepsilon_r - \cos^2\psi')/\chi \ .$$

G is a ground wave attenuation function similar to F. q and b' are generally termed the numerical distance and phase factor respectively for horizontal dipoles. In Eqs. (8) and (10)-(14) surface waves terms can be identified by the presence of F or G as a factor. Eqs. (8) and (10)-(15) including higher order terms were programmed for the Datacraft 6024 digital computer. Subroutine DIPOLE is described in Appendix I.

We now wish to investigate the nature of the ground wave attenuation functions. Since they are similar we will look only at F. Combining Eqs. (9d-f) we have

$$(16) \qquad w \approx \frac{4\pi\cos(b)\, e^{-jb}}{(1-R_v)^2} \frac{R_2}{\lambda\chi} \ .$$

If we consider a point in the far-field and at a low elevation angle, α, such that $R_2 \gg (z+a)$, then from Eqs. (9a,b) we have $R_v \approx -1$ and

$$(17) \qquad w \approx \pi\cos(b)\, e^{-jb} \frac{R_2}{\lambda\chi} \ .$$

Inserting the value of χ from Eq. (3) into Eq. (17) we have

$$(18) \qquad w \approx \pi\cos(b)\, e^{-jb} \frac{R_2 f_{kc}}{1.8\times10^{18}\lambda\sigma} \ .$$

For frequencies near 200 MHz, and a typical ground conductivity of 10^{-13} emu, w will be on the order of R_2 (meters) in magnitude. From Eq. (9g) we see $0 \leq b \leq \pi/2$ and thus $-\pi/2 \leq \arg w \leq 0$. Thus, the argument of the complementary error function of Eq. (9c) is a complex number whose phase is between $\pi/4$ and $\pi/2$. Its magnitude may be evaluated exactly using Eq. (18), but for frequencies around 200 MHz and for typical ground constants (i.e., $\epsilon_r \approx 5$, $\sigma \approx 10^{-13}$ emu) its magnitude is on the order of $\sqrt{R_2} \approx \sqrt{R}$ (meters). In this case the following asymptotic expansion for $\mathrm{erfc}(z = j\sqrt{w})$ is valid[11]

$$\sqrt{\pi}\, z\, e^{z^2}\, \mathrm{erfc}(z) \sim 1 + \sum_{m=1}^{\infty} \frac{1 \cdot 3 \cdots (m-1)}{(2z^2)^m} \quad . \tag{19}$$

Retaining only the first term of the summation we have

$$\sqrt{\pi}\, z\, e^{z^2}\, \mathrm{erfc}(z) \sim 1 + 1/2z^2. \tag{20}$$

If in Eq. (9c) we make the change of variables $j\sqrt{w} = z$ we get

$$F = [1 - \sqrt{\pi}\, z\, e^{-z^2}\, \mathrm{erfc}(z)]. \tag{21}$$

Combining Eqs. (20) and (21) we get finally the well known result

$$F \sim -1/2z^2 \approx \text{constant}/R. \tag{22}$$

Since surface wave terms vary as F/R or G/R we then see that they have a $1/R^2$ distance dependence for VHF frequencies and typical ground constants.

We next wish to consider the far-field space wave at low elevation angles. Noting that $\cos\psi'' \approx \cos\psi' \approx 1$, and $R_v \approx -1$, the space wave portion of Eq. (8) becomes

$$E_z^v(\text{space}) = -jk \left(\frac{e^{-jkR_1}}{R_1} - \frac{e^{-jkR_2}}{R_2} \right) \quad . \tag{23}$$

We can write R_2 in terms of R_1 using the approximation

$$R_2 \approx R_1 + \Delta R = R_1 + 2a\sin\alpha \approx R_1 + 2a\alpha. \tag{24}$$

Combining Eqs. (23) and (24) and using $1/R_1 \approx 1/R_2 \approx 1/R$ we get

$$(25) \qquad E_z^V \text{ (space)} \approx 2ak\, e^{-jkR_1} \left(\frac{a}{R}\right) \quad .$$

Thus, for a given elevation angle a the space wave has the usual 1/R dependence, and we would expect it to predominate the surface wave except at elevation angles so small that a is on the order of or smaller than 1/R. Eq. (25) also predicts that the space wave field strength should increase with increasing elevation angle or increased height of the vertical dipole from the earth's surface. Right on the earth's surface, where $a = 0$, the space wave vanishes and all radiation is due to the surface wave. Summarizing we see that the surface wave predominates at very low elevation angles, and the space wave at the higher elevation angles.

From the above discussion we do not mean to imply that the peak magnitude of the surface wave field is always considerably less than the peak magnitude of the space wave field. The numerical distance can be related to $|F|$ or $|G|$ and can thus be a measure of the relative importance of the surface wave. In Fig. 3 is plotted the

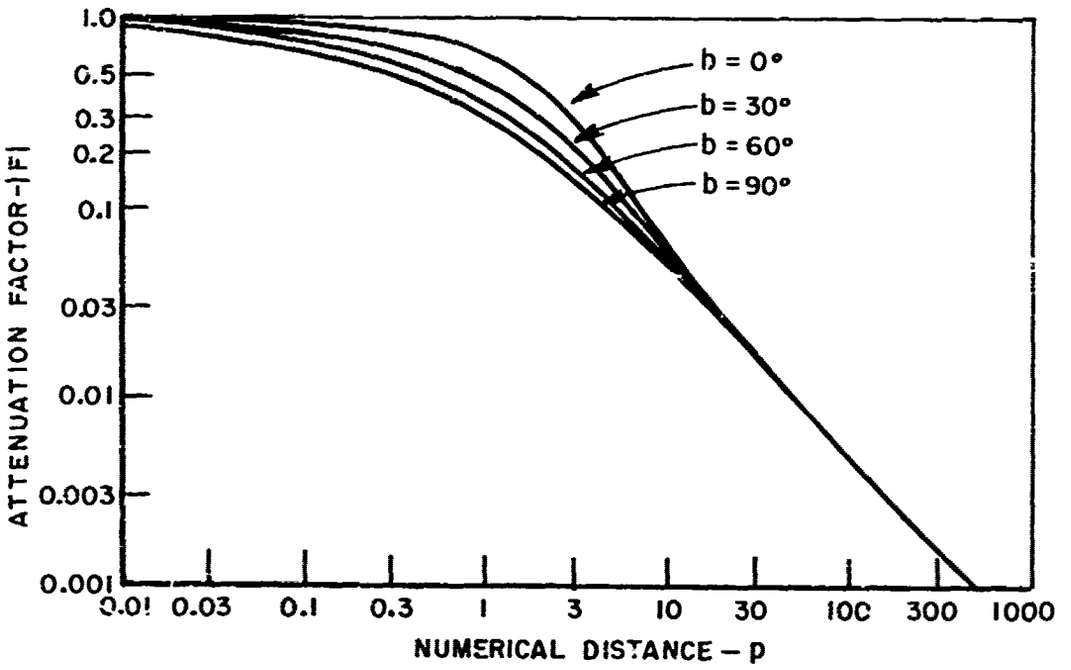

Fig. 3. The absolute value of the ground wave attenuation function for vertical dipoles versus the numerical distance.

absolute value of the ground wave attenuation function, $|F|$, versus p, the numerical distance for vertical dipoles, and we see that for $p > 10$, $|F| \approx 1/2p$[14]. Thus the surface wave is less important for larger values of p. If we consider the example

$f = 200$ MHz,
$R = 1$ km, and
$\sigma = 10^{-12}$ emu,

then we have $p \approx 250 \cos(b)$, and from Fig. 3 $|F| \approx 0.002$. However, if we consider the same example but with $f = 1$ MHz we have $p \approx .005 \cos(b)$ and $|F| \approx 1.0$. The horizontally polarized surface wave is generally attenuated more rapidly than the vertical polarization. Jordon and Balmain[14] present a good discussion of the effects of the ground constants, frequency, and range on the pattern of infinitesimal electric current elements.

III. NUMERICAL PARAMETER STUDY

A. Introduction

In this section we wish to look at the far-field power patterns of the basic radiating elements, which are the horizontal and vertical infinitesimal electric current elements. The element patterns were calculated for the planes shown in Fig. 4. Due to symmetry only the first 90° of the pattern in the xz plane will be shown for the vertical element. Patterns for the horizontal element, assumed to be aligned with the x axis, will be shown for the first 90° of the plane containing the dipole axis and the plane perpendicular to the dipole axis, i.e., the xz and yz planes respectively.

The pattern for an antenna over a lossy earth is dependent upon many factors. Some of the most important are:

1. Radial distance from the source.
2. Geometry of the antenna, and the antenna height from the surface.
3. Conductivity and permittivity of the lossy ground.
4. In a practical sense, the vegetation, buildings, vehicles, etc.

Clearly it is impractical to show the influence of the first three parameters each time an antenna pattern is displayed and virtually impossible to account for the fourth. Thus, we wish to do a parameter study on the infinitesimal electric current element to obtain a qualitative indication for the effects of the first three parameters on real antennas. Buildings, vegetation, hills, and other obstacles

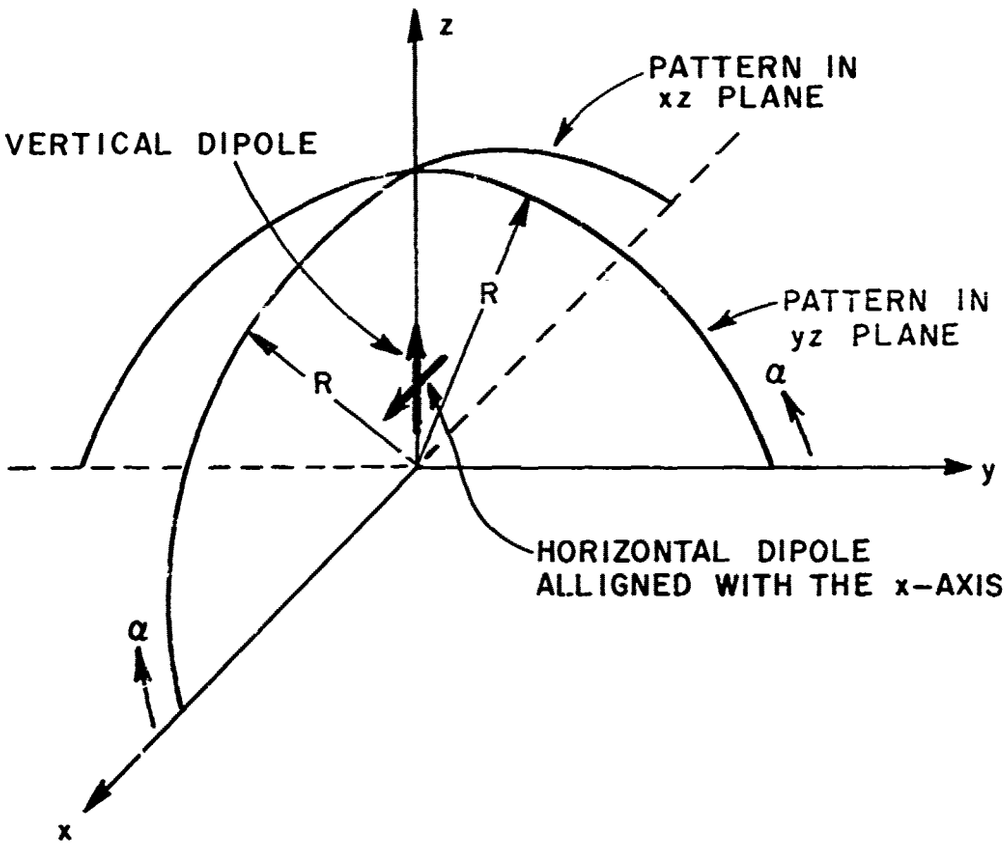

Fig. 4. Geometry for patterns.

effect an antenna's pattern in two ways. They may either scatter or absorb some of the energy radiated by the antenna, and this scattering or absorption may have a much greater effect on an antenna's pattern than any or all of the first three parameters. Not knowing the geometry of the obstacles one can only assume that the amount of radiation received at one point from a source located at another point is directly proportional to the amount of radiation received in the absence of the obstacles. This is our justification for studying the problem of propagation over an infinite flat lossy earth. Stated another way, we wish to show the effect of the lossy earth on an antenna's pattern, while we understand that in practice there are other factors, (i.e., scattering or absorbing obstacles) affecting the pattern. Unless it is one of the parameters being varied, patterns will be shown for R = 1 km, $\varepsilon_r = 5$, $\sigma = 3 \times 10^{-13}$ emu = 0.03 mho/meter, and f = 162 MHz. A log log scale was chosen to display this data because it emphasizes the low elevation angles of

interest in this study and provides for a good dynamic range. For each of the three parameter studies the patterns are normalized such that the largest peak power for any curve shown, within a particular parameter study, is unity. Thus, even though a particular study may contain many graphs, each having many curves, any two curves may be compared directly.

The pattern calculations in the following sections were made using subroutine DIPOLE described in Appendix I. Subroutine DIPOLE includes the effects of space waves and surface waves, even though for many of the calculations only the space wave is significant. In these cases much effort may be saved by using only the first two terms in Eqs. (8) and (10)-(14).

B. Pattern Radius

In this and in following sections various far-field power patterns will be given for R = 1 km. If these patterns are assumed to apply to other radii by simply introducing the usual $1/R^2$ power dependence some error will be incurred, especially for low elevation angles. Using the $1/R^2$ dependence essentially amounts to ignoring the surface wave and assuming the space wave predominates. As was seen in Section II, this approximation will be valid except at low elevation angles. Figures 5, 6 and 7 have been drawn to obtain an idea of the nature of this error. The two curves of Fig. 5 are the relative errors in extrapolating from 1 km to 0.1 km or 1 km to 10 km using a $1/R^2$ power dependence for a vertical dipole located $\lambda/4$ above a ground with $\epsilon_r = 5$, $\sigma = .03$ mho/meter $= 3 \times 10^{-13}$ emu, and f = 162 MHz. If P_a is the power at R_a and some elevation angle, and P_b is the power at R_b and the same elevation angle, then the relative error in extrapolating from R_a to R_b is given by

$$(26) \qquad E = \left[P_b - \left(\frac{R_a}{R_b} \right)^2 P_a \right] \Big/ P_b .$$

Figures 5-7 were drawn by calculating the error exactly (i.e., using subroutine DIPOLE) every 0.1° from 0.1° to 1.0° and every degree from 1° to 10°. The error at any point is not only a function of the relative magnitude of the space and surface waves, but also of their relative phases. Thus, at a point where the space and surface waves add in the proper phase the error may be considerably less than at nearby points. This accounts for the sometimes erratic nature of the curves in Figs. 5-7.

In Fig. 5 we see that it is possible to extrapolate from 1 to 0.1 km with a relative error less than 1% for elevation angles greater than 6°, while extrapolation from 1 to 10 km can be done with a relative error less than 1% for elevation angles greater than 2°. Figures 6 and 7 are identical to Fig. 5 except that they are for horizontal dipoles

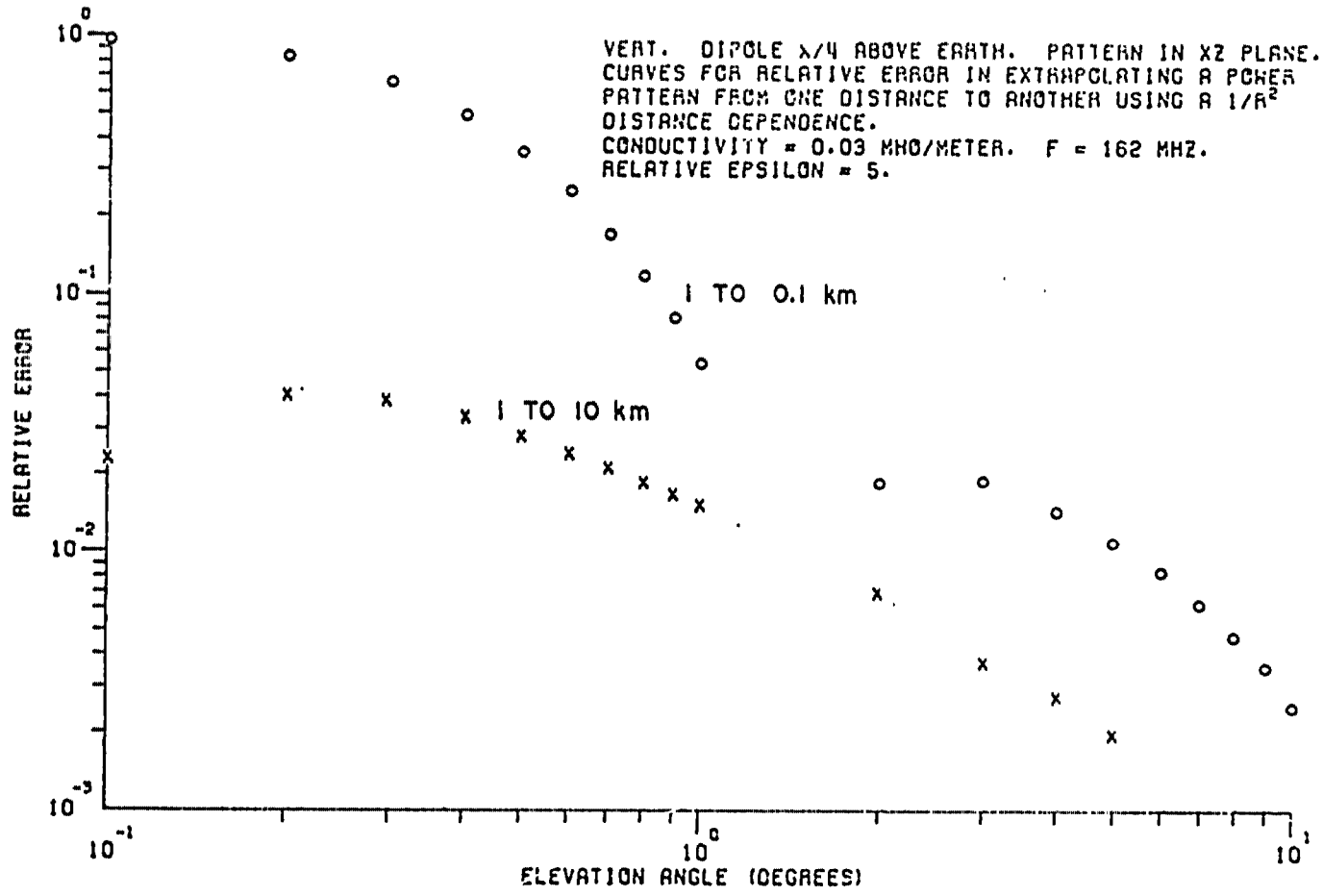

Fig. 5. Typical extrapolation error for vertical dipoles.

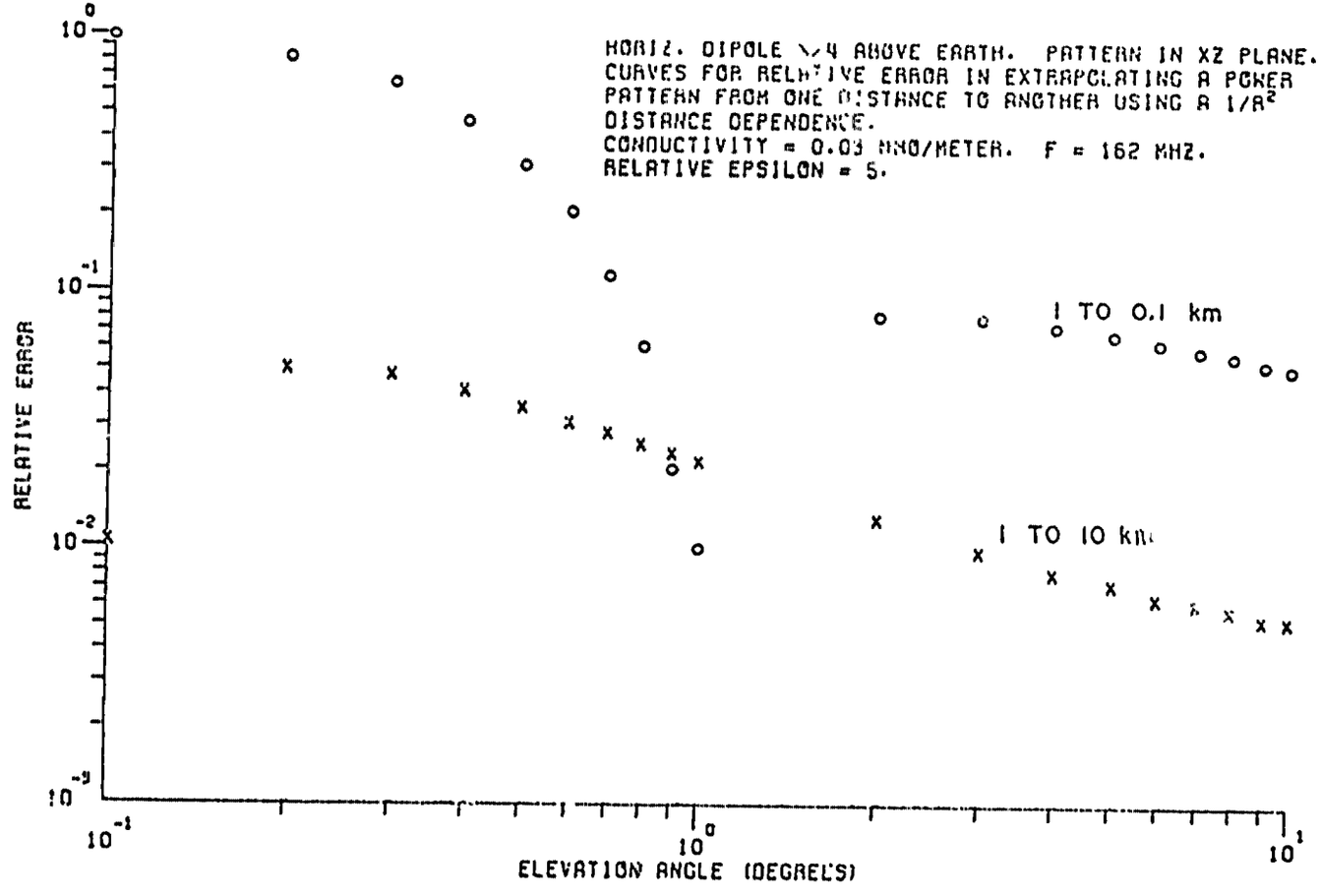

Fig. 6. Typical extrapolation error for horizontal dipole in the xz plane.

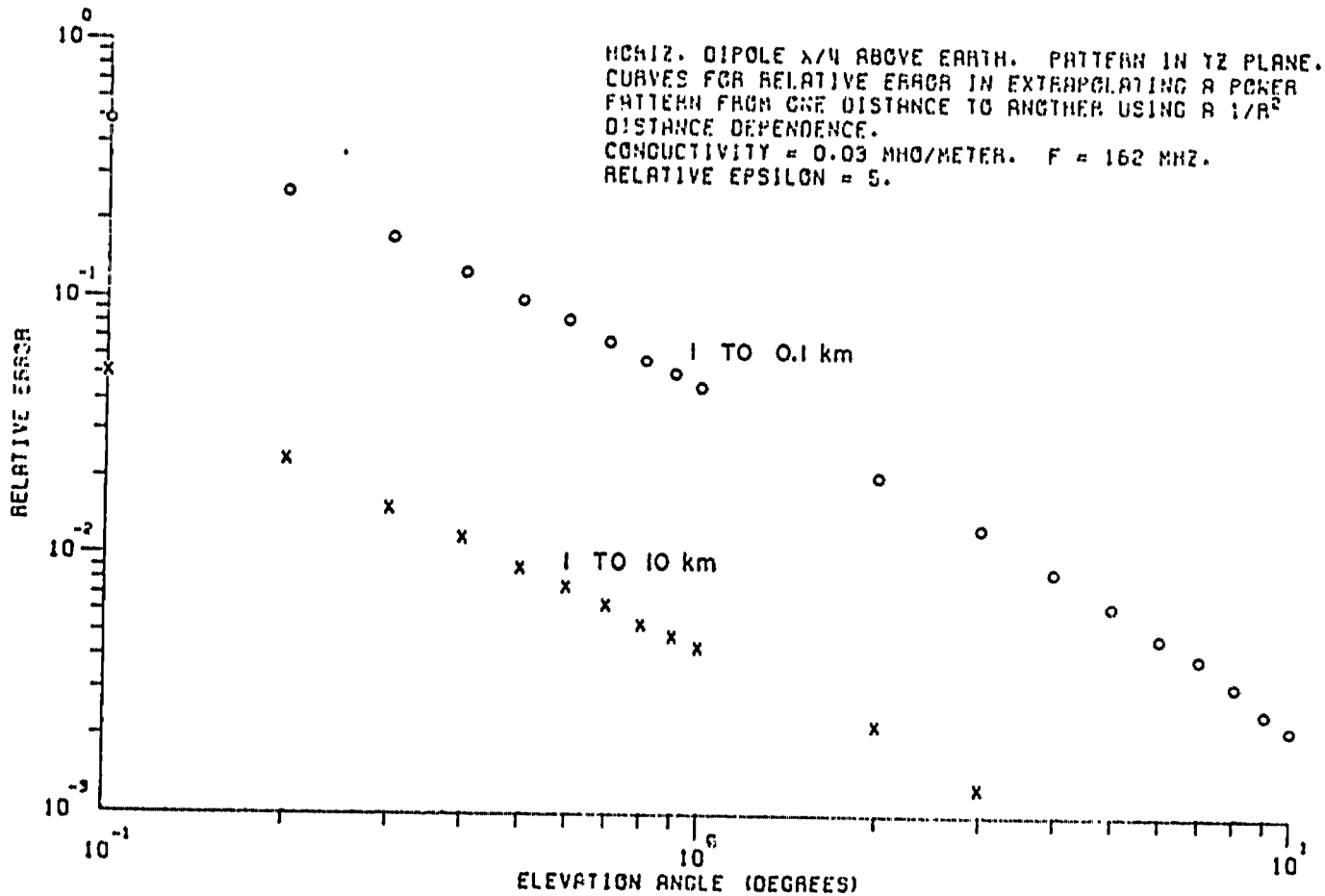

Fig. 7. Typical extrapolation error for horizontal dipole in the yz plane.

with the pattern in the xz and yz planes respectively. Note in Figs. 5-7 that extrapolation to greater radii is done more accurately than to shorter radii. This is because the surface wave, which is the cause of the error, is less significant at greater distances.

C. Dipole Orientation and Height from Surface

Here we wish to obtain an indication of the type of pattern radiated by the infinitesimal vertical dipole and the horizontal dipole in either plane. We also desire to determine the effect of elevating the dipoles from the earth's surface.

In Fig. 8 curves are shown for the vertical element, and Figs. 9 and 10 contain curves for the horizontal element in the xz and yz planes respectively. We note the following from Figs. 8-10.

1. As one would expect, the vertical elements are the best radiators at low elevation angles, and this is especially true when the elements are less than $\lambda/2$ from the earth's surface. The horizontal elements radiate best at very large elevation angles.

2. Except for the horizontal dipole in the xz plane, which is the poorest radiator at low elevation angles, raising the element from the earth's surface greatly increases the amount of radiation at low elevation angles.

3. The radiation from an elevated element is the sum of radiation from the source and its image. Thus, raising the element makes the source look larger and sidelobes appear in the patterns.

In Fig. 11 we plot the elevation angle corresponding to the first pattern maximum versus the dipole height. Note that for the vertical element, and the horizontal element in the yz plane it is possible to shift this maximum well under 2° by elevating λ or more, while the peak of the pattern for the horizontal element in the xz plane is never less than 40°.

Figures 8-10 can be used as qualitative design information since the fields of an extended source is simply an integration or summation of the fields of infinitesimal sources. For example, if one wants to design an antenna to radiate at low elevation angles, and is restricted to placing his antenna very near the earth's surface, then he should rely on vertical wires. However, if radiation at high elevation angles is desired, then horizontal wires should be used.

As a second example assume one has the pattern for a horizontal linear antenna located $\lambda/2$ above the earth in the plane containing the antenna axis. It is desired to find the effect of lowering the antenna almost to the earth's surface. From Fig. 10 we see that this will seriously degrade the antenna's performance, especially at the lower elevation angles.

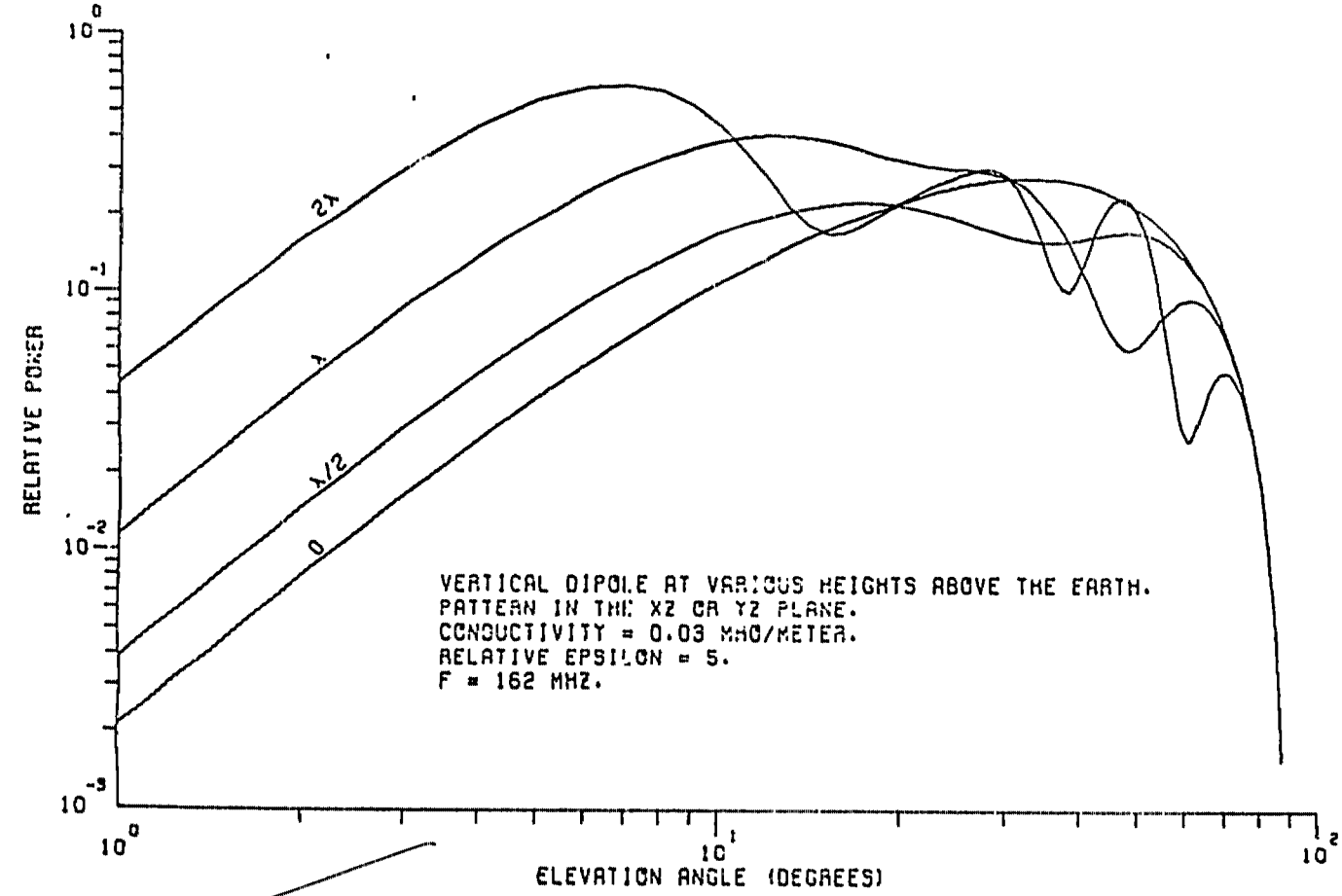

Fig. 8. Patterns for vertical dipole versus the dipole height.

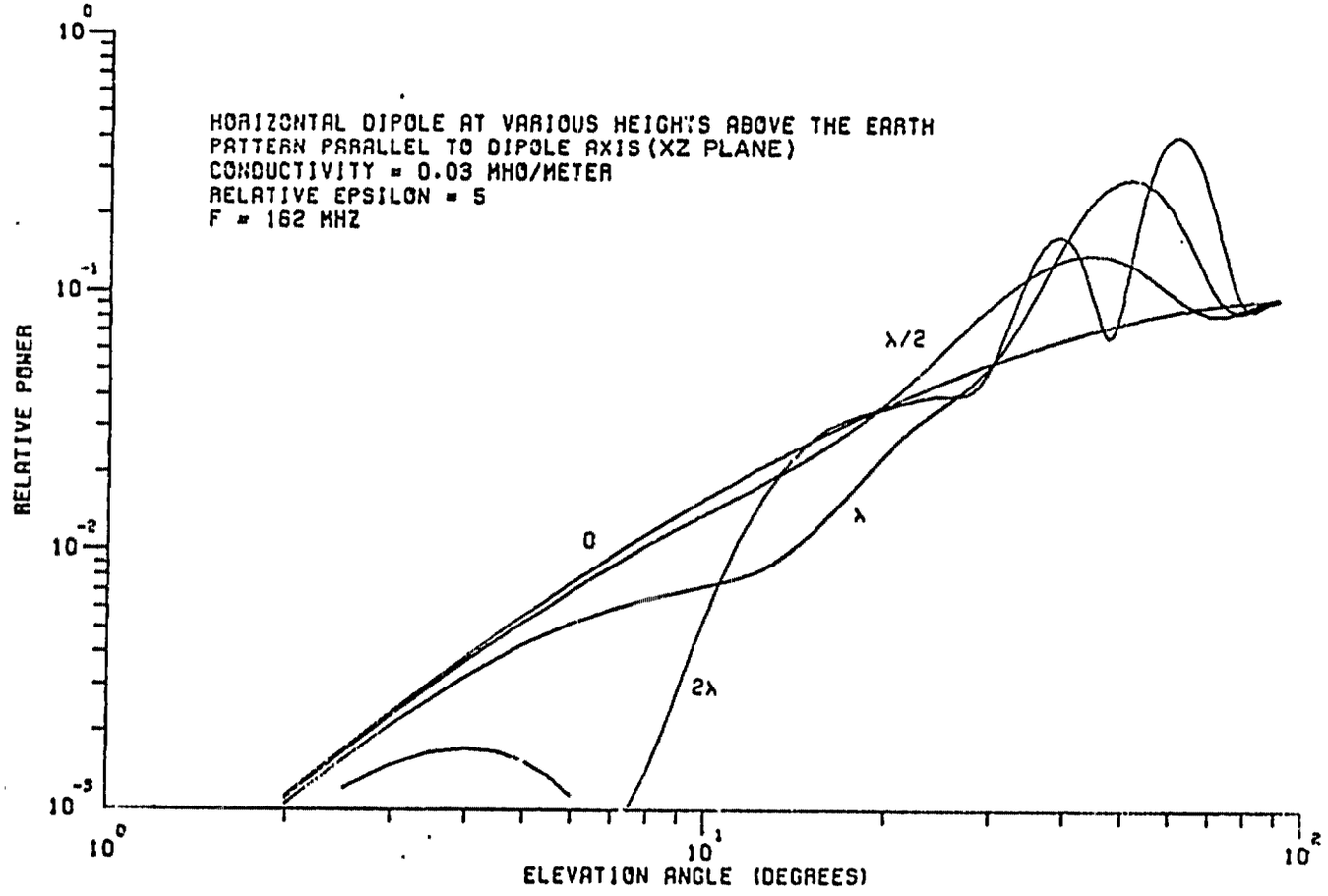

Fig. 9. Patterns for horizontal dipole in the xz plane versus the dipole height.

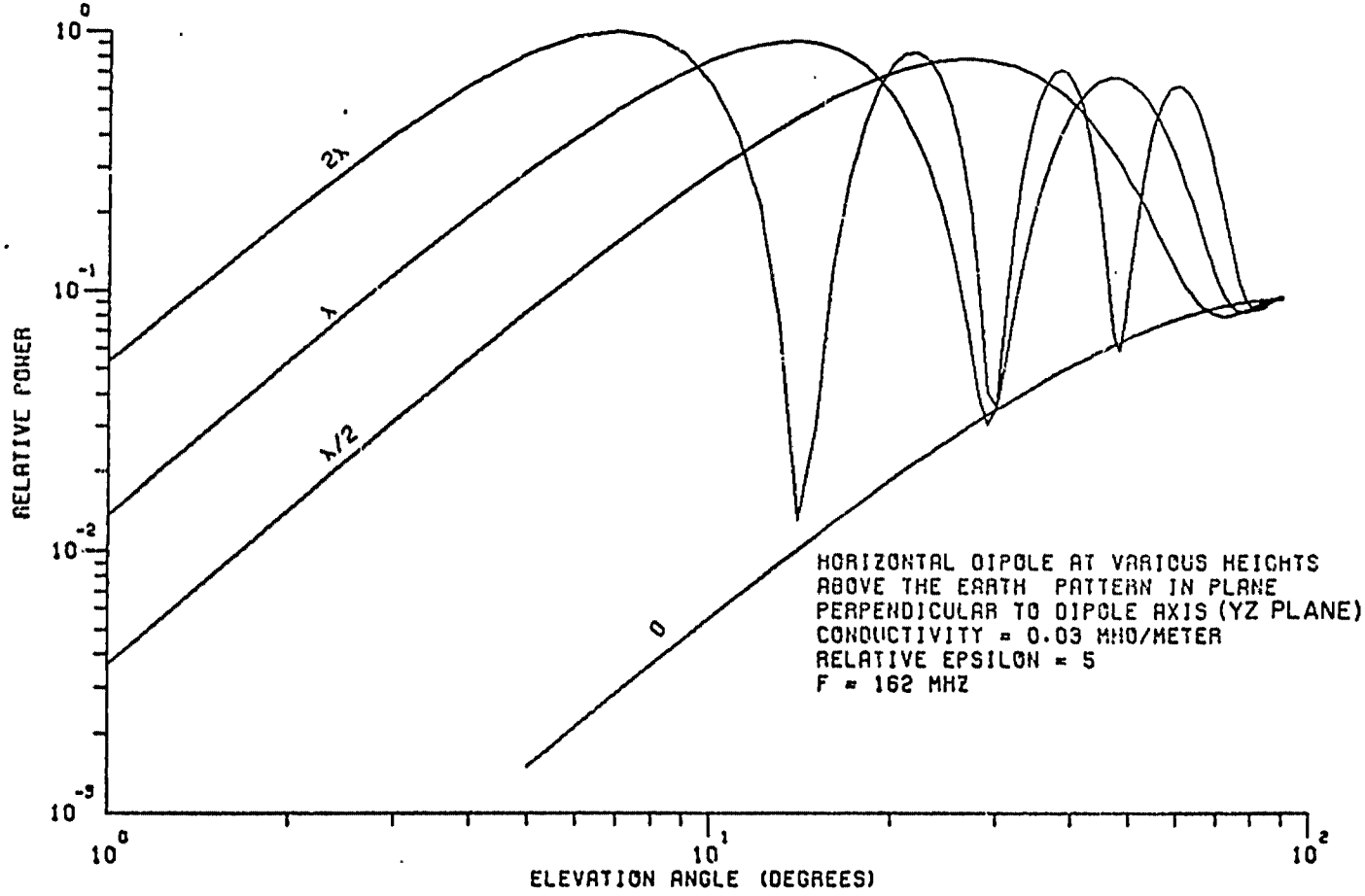

Fig. 10. Patterns for horizontal dipole in the yz plane versus the dipole height.

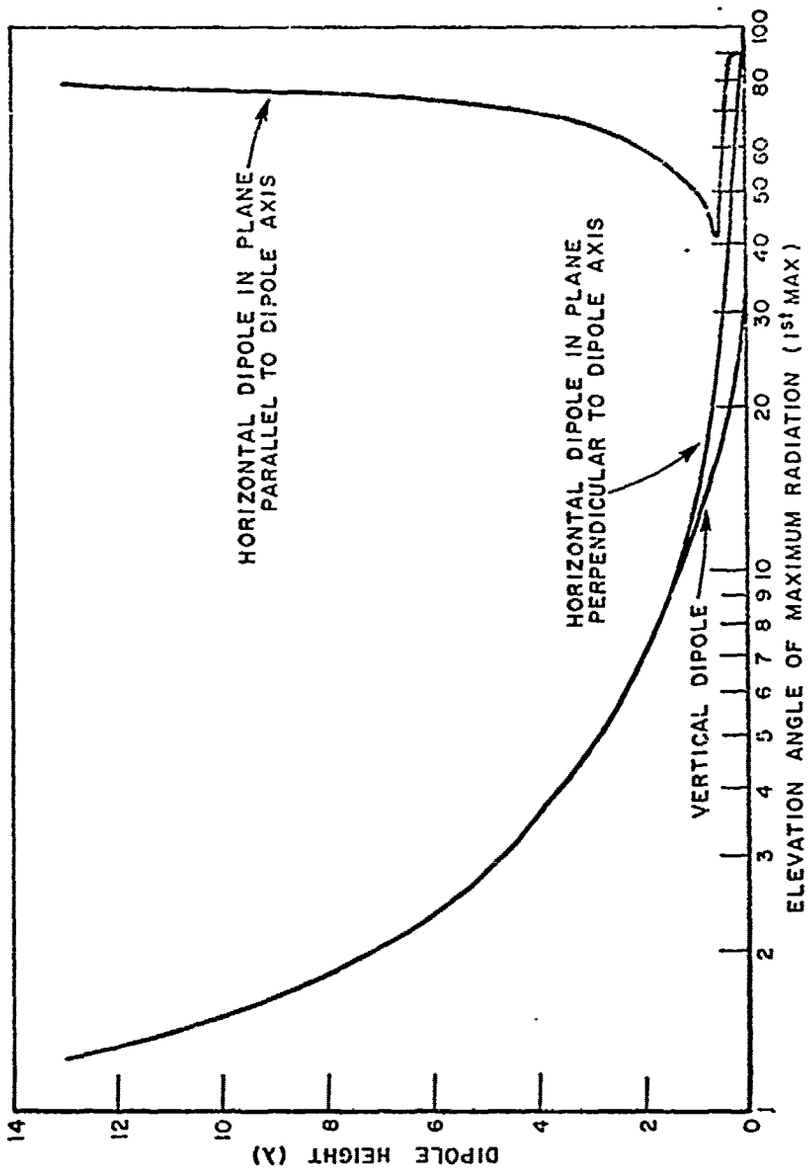

Fig. 11. Angle of pattern maximum nearest the ground versus the dipole height.

D. Ground Constants

Here we wish to determine the effects on a power pattern of varying the permittivity and the conductivity of the earth. The range of ground constants covered is ϵ_r = 2 to 32 and σ = 10^{-12} to 10^{-15} emu or 0.1 to 0.0001 mho/meter. All curves are for the infinitesimal dipoles located $\lambda/4$ above the earth's surface and at R = 1 km. Figure 12 is for the specific case of a vertical dipole, σ = 10^{-12} emu, and curves are drawn for ϵ_r = 2, 4, 8, 16, and 32. Figures 13-15 are identical to Fig. 12 except that σ = 10^{-13}, 10^{-14}, and 10^{-15} emu respectively. Figures 16-19 are identical to Figs. 12-15 respectively except that they are for a horizontal dipole with the pattern in the xz plane, and Figs. 20-23 are identical to Figs. 16-19 except that they are for a horizontal dipole in the yz plane.

Note that in Figs. 12-23 varying σ over 3 orders of magnitude has almost no effect on the patterns, while varying ϵ_r from 2 to 32 does significantly alter the patterns especially for the vertical dipole. Increasing ϵ_r increases the radiation at low elevation angles for vertical dipoles, and decreases the radiation at low elevation for horizontal dipoles. The radiation from horizontal dipoles at large elevation angles is increased as ϵ_r is increased.

Figures 12-23 could be used if one knew for example the pattern of a vertical linear antenna over a ground with $\epsilon_r \approx 4$ and $\sigma \approx 10^{-13}$ emu, and it was desired to qualitatively predict its performance if it were located over a ground with $\epsilon_r \approx 10$ and $\sigma \approx 10^{-15}$ emu. Then using Figs. 12 and 14 we see that the power at low elevation angles will be increased slightly, while that at large elevation angles will be essentially unchanged.

IV. REPRESENTING CONTINUOUS CURRENT DISTRIBUTIONS BY A FINITE NUMBER OF INFINITESIMAL SOURCES

In this section we wish to devise a method for determining the fields radiated by an arbitrary current distribution in terms of a finite summation of the fields of infinitesimal sources rather than by an integration over the source distribution. Consider the wire in Fig. 24a which is assumed to carry the arbitrary current distribution $\vec{I}(\vec{R}')$. The fields of this current distribution at the field point $\vec{R}$ can be expressed using the following linear vector function

$$(27) \qquad \vec{E}(\vec{R}) = \int_{\text{wire}} \vec{I}(\vec{R}') \cdot \vec{\vec{A}}(\vec{R}-\vec{R}')\, d\ell$$

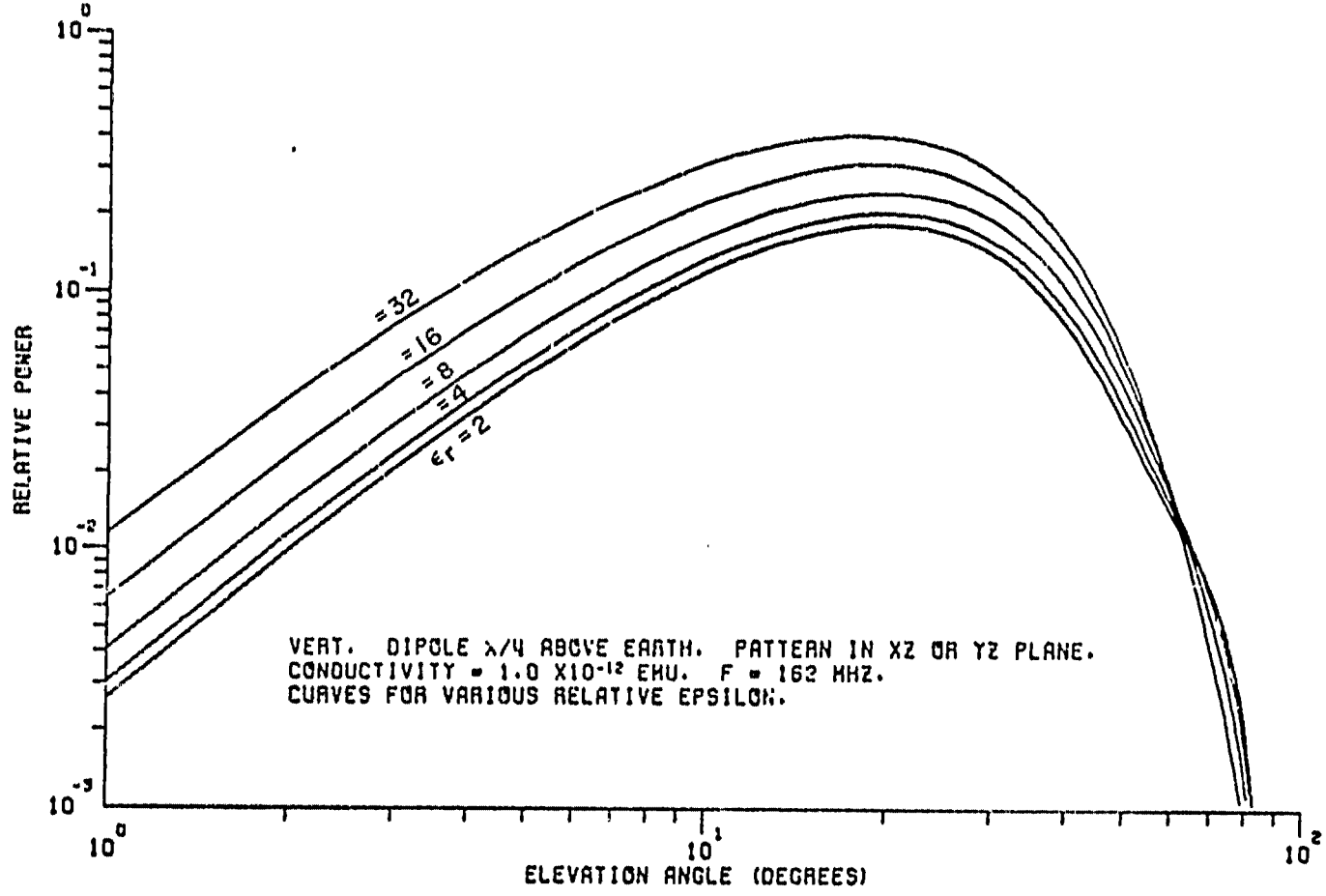

Fig. 12. Patterns for vertical dipole with σ=10^{-12} emu vs. ϵ_r.

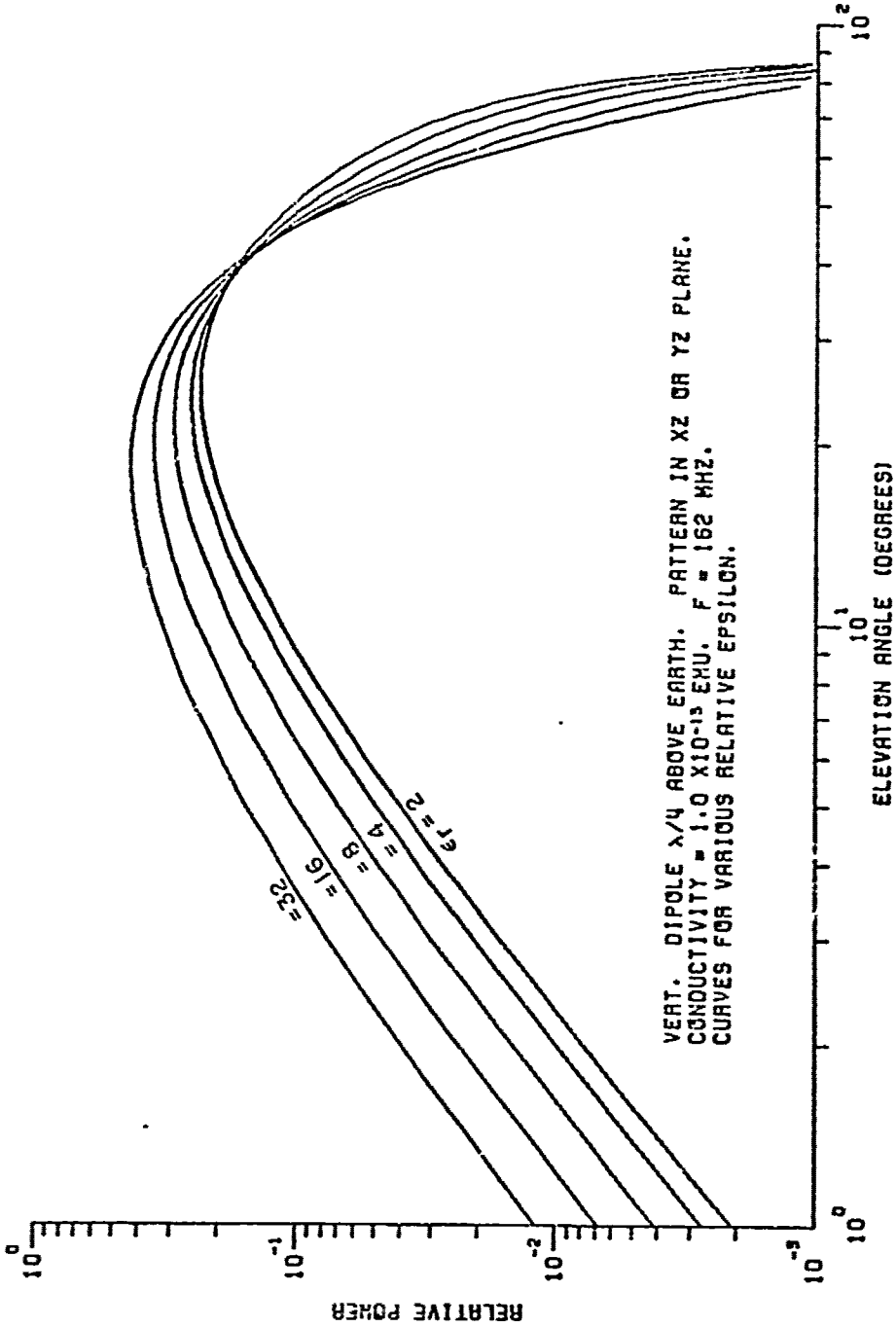

Fig. 13. Patterns for vertical dipole with $\sigma=10^{-13}$ emu versus ε_r.

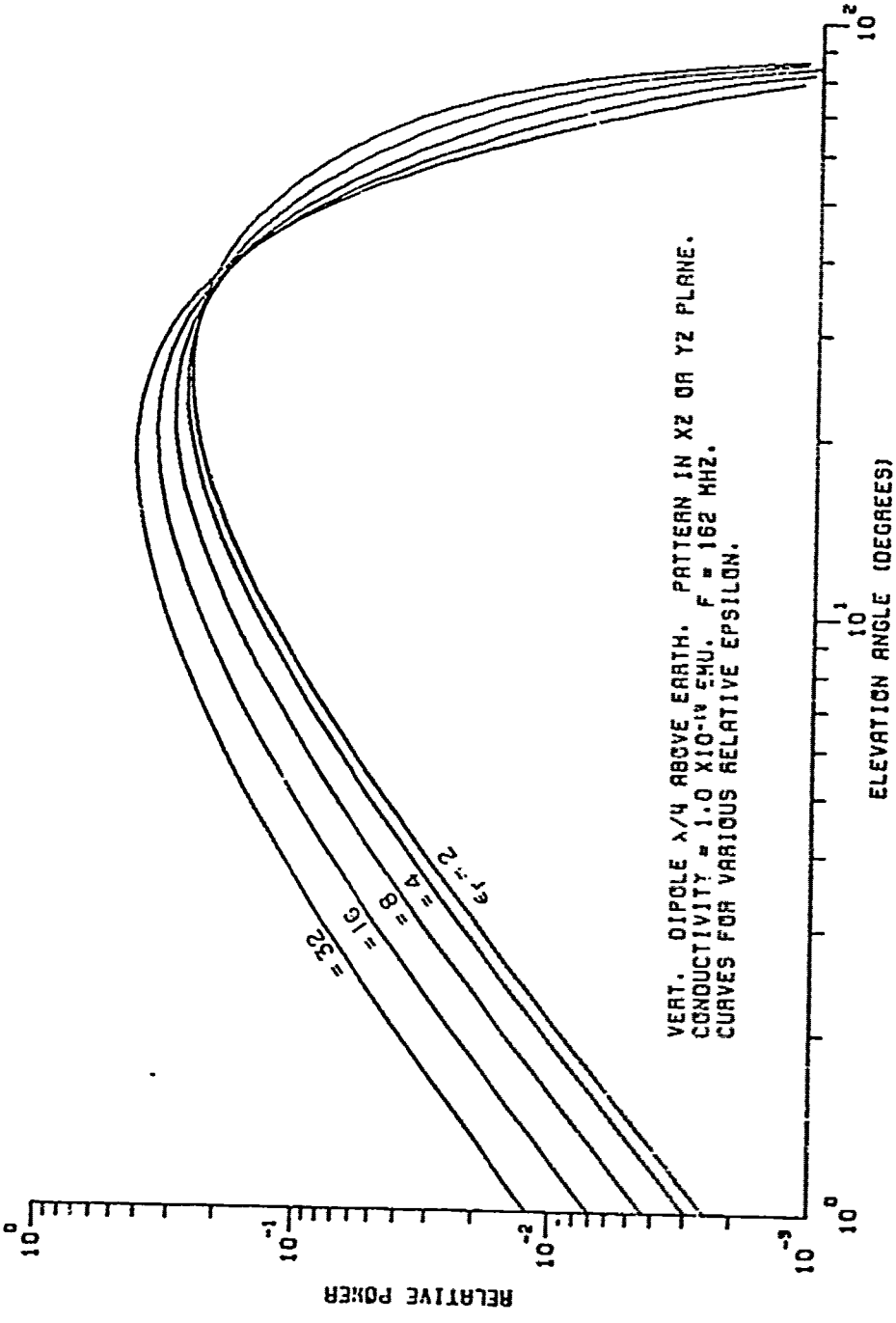

Fig. 14. Patterns for vertical dipole with $\sigma=10^{-14}$ emu versus ε_r.

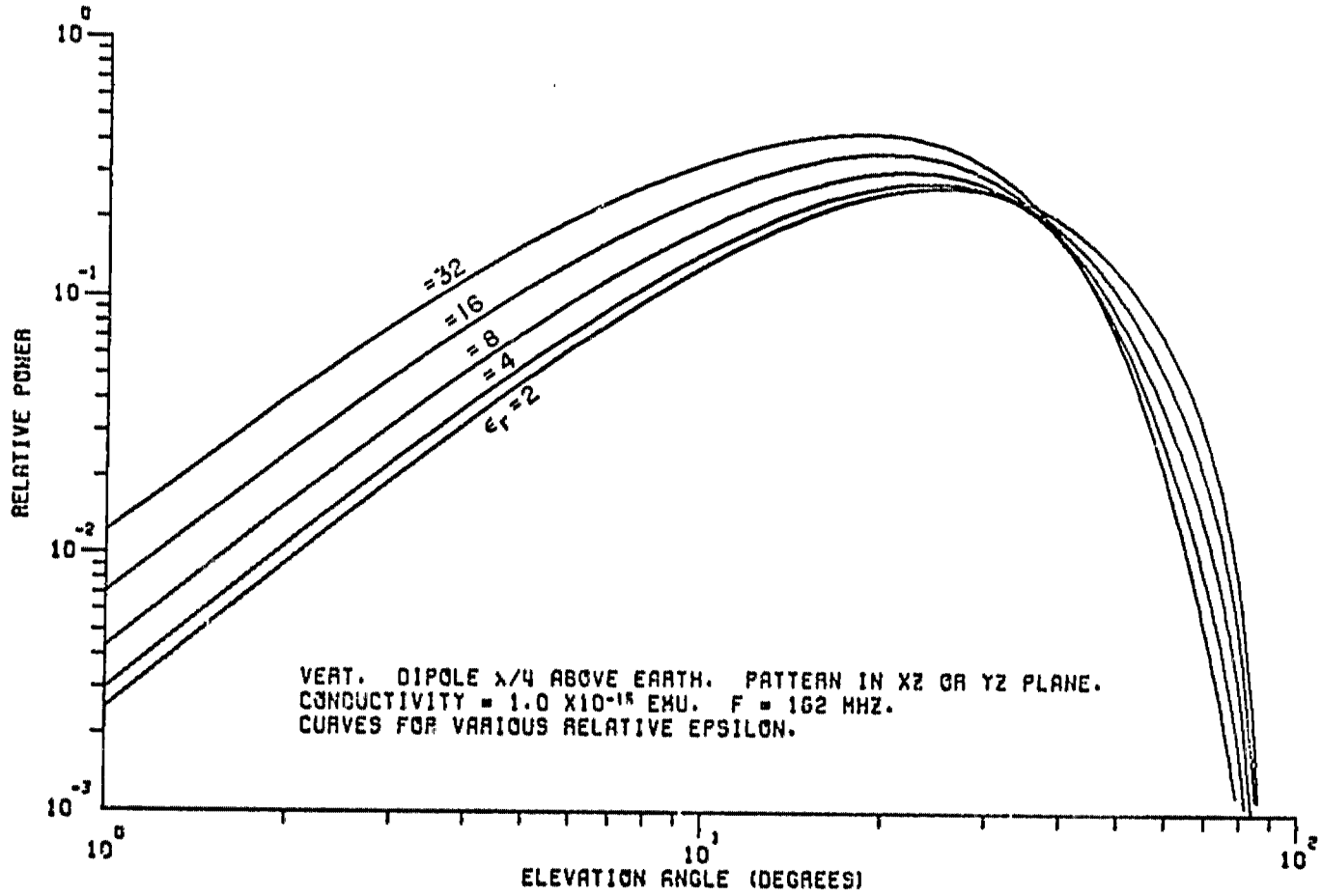

Fig. 15. Patterns for vertical dipole with $\sigma=10^{-15}$ emu versus ϵ_r.

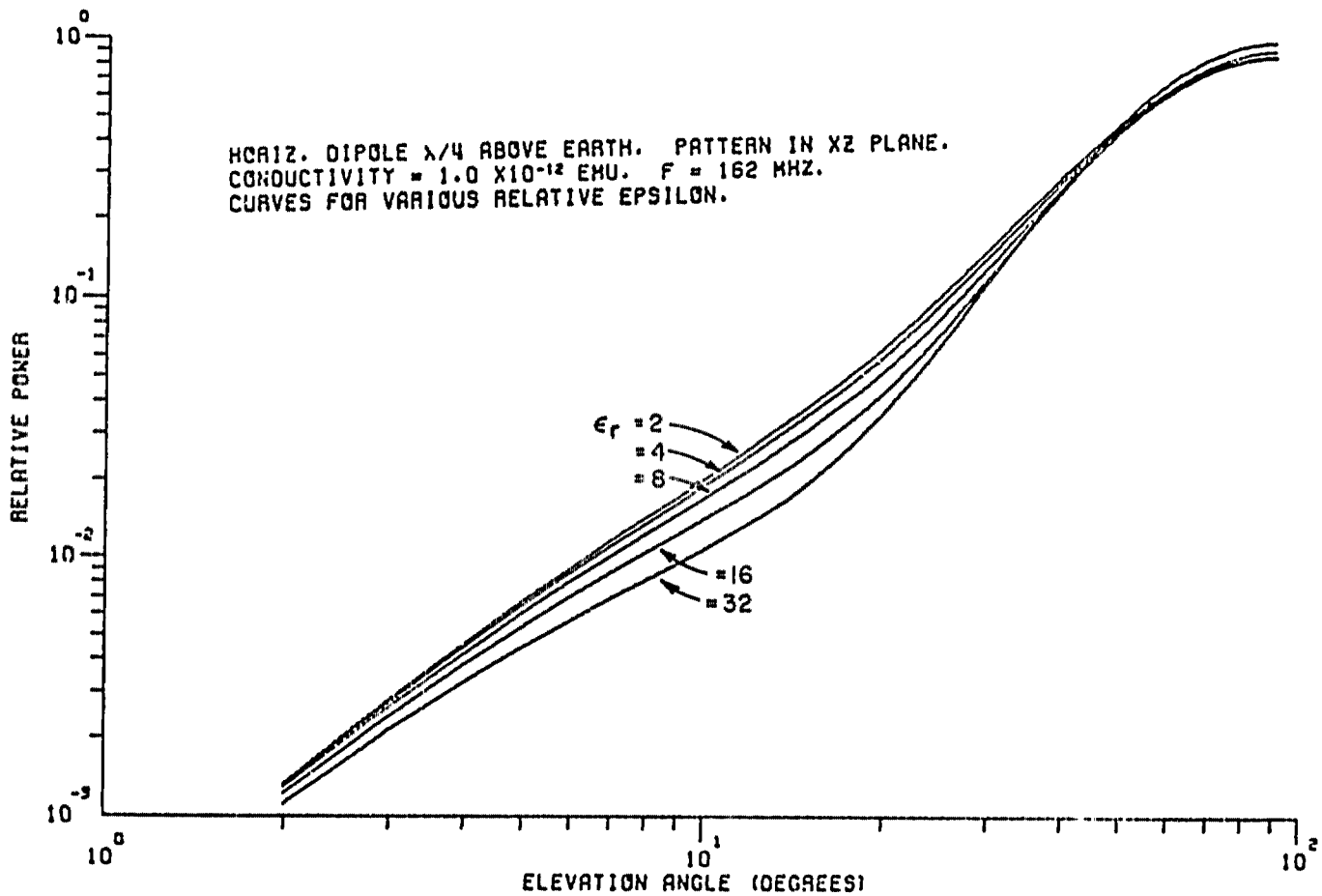

Fig. 16. Patterns for horizontal dipole in the xz plane with $\sigma=10^{-12}$ emu versus ϵ_r.

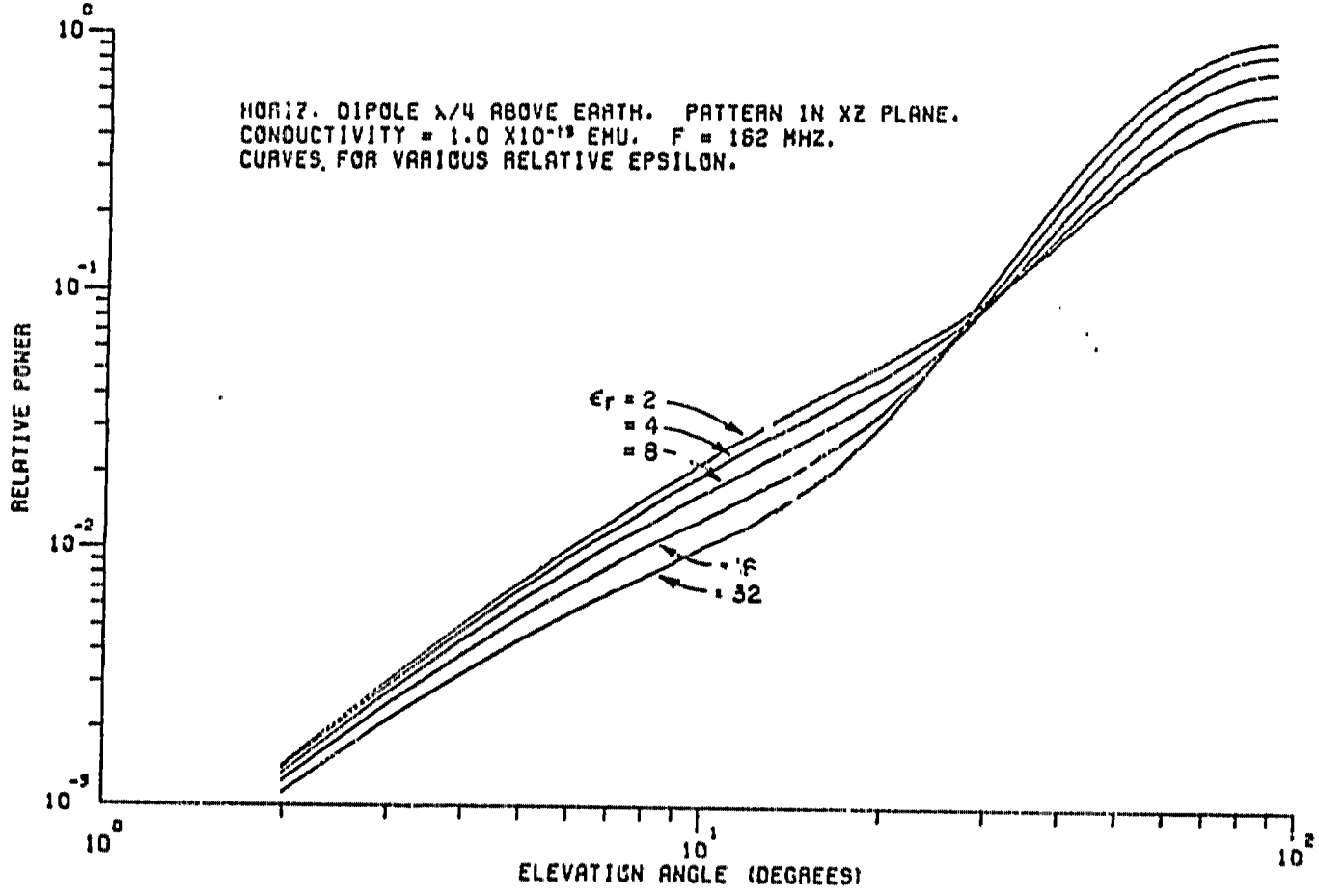

Fig. 17. Patterns for horizontal dipole in the xz plane with $\sigma=10^{-13}$ emu versus ϵ_r.

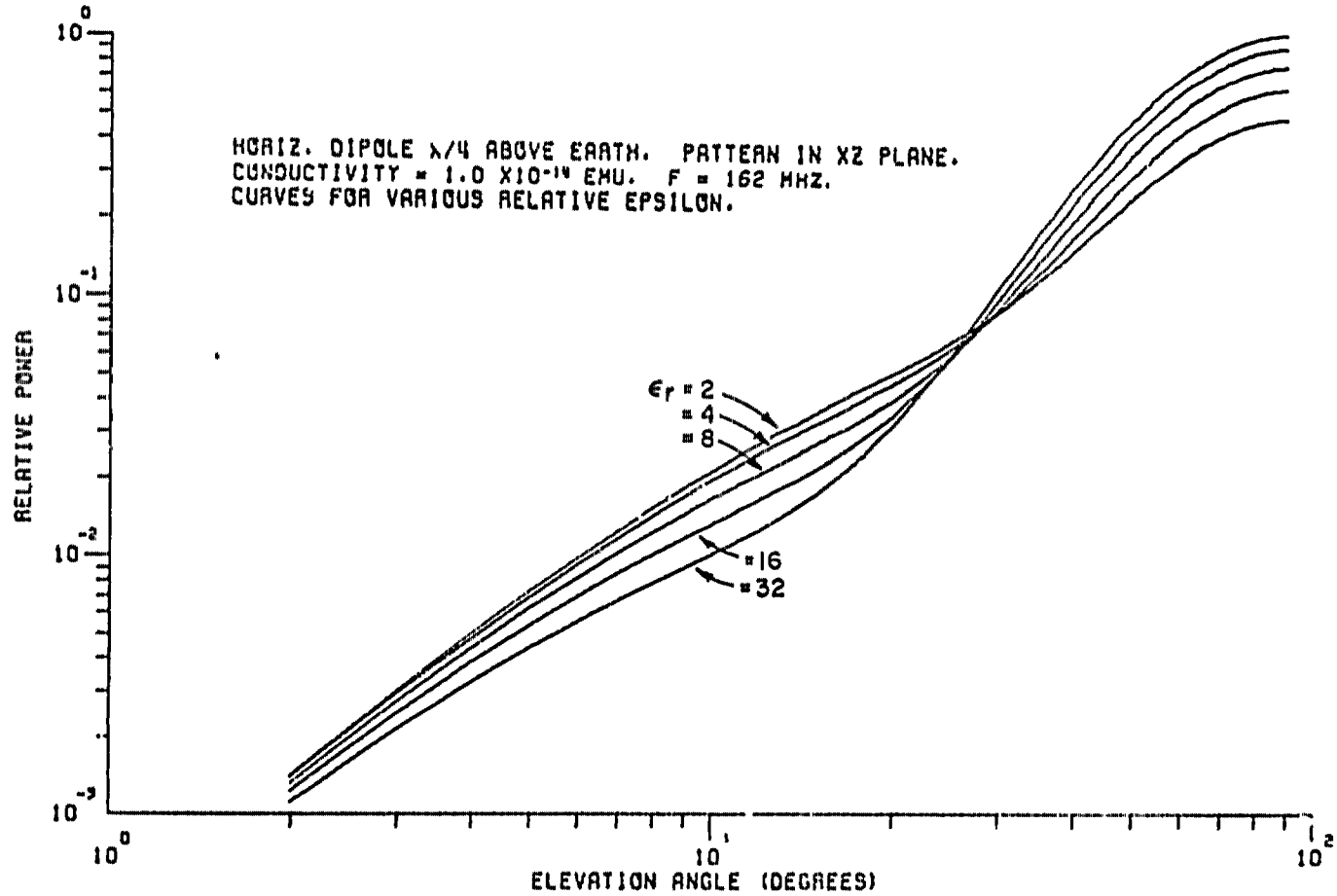

Fig. 18. Patterns for horizontal dipole in the xz plane with $\sigma=10^{-14}$ emu versus ε_r.

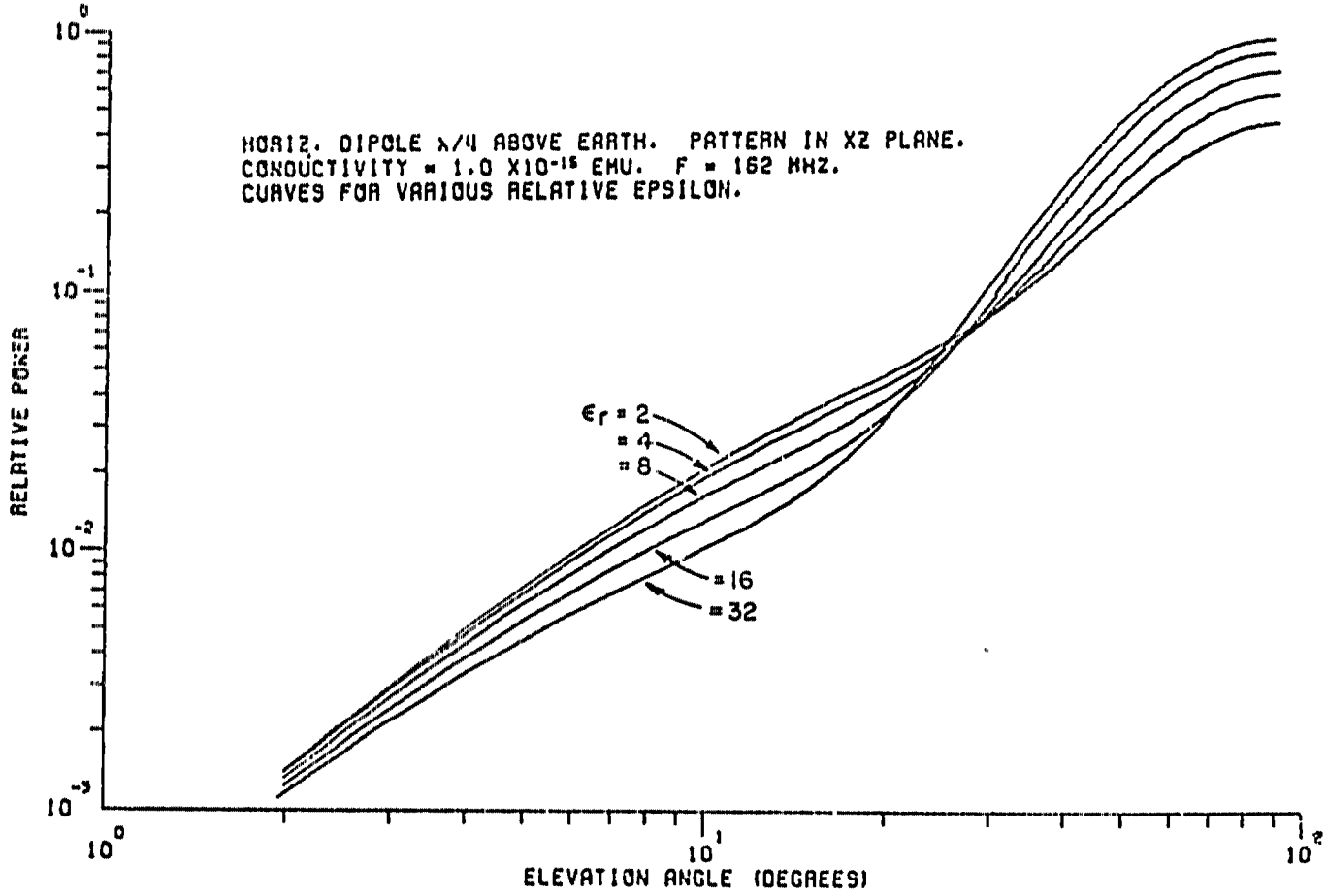

Fig. 19. Patterns for horizontal dipole in the xz plane with $\sigma=10^{-15}$ emu versus ϵ_r.

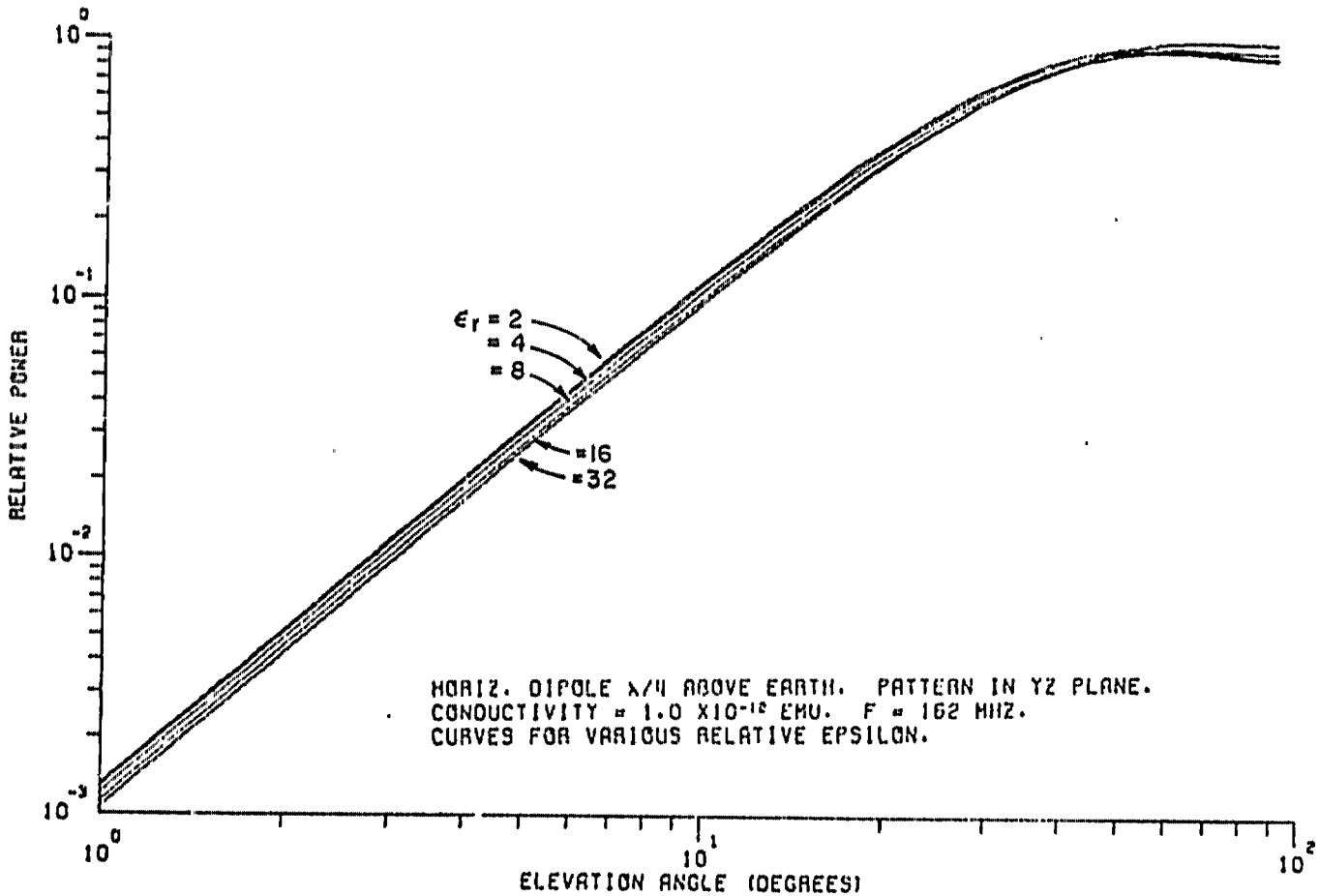

Fig. 20. Patterns for horizontal dipole in the yz plane with $\sigma=10^{-12}$ emu versus ϵ_r.

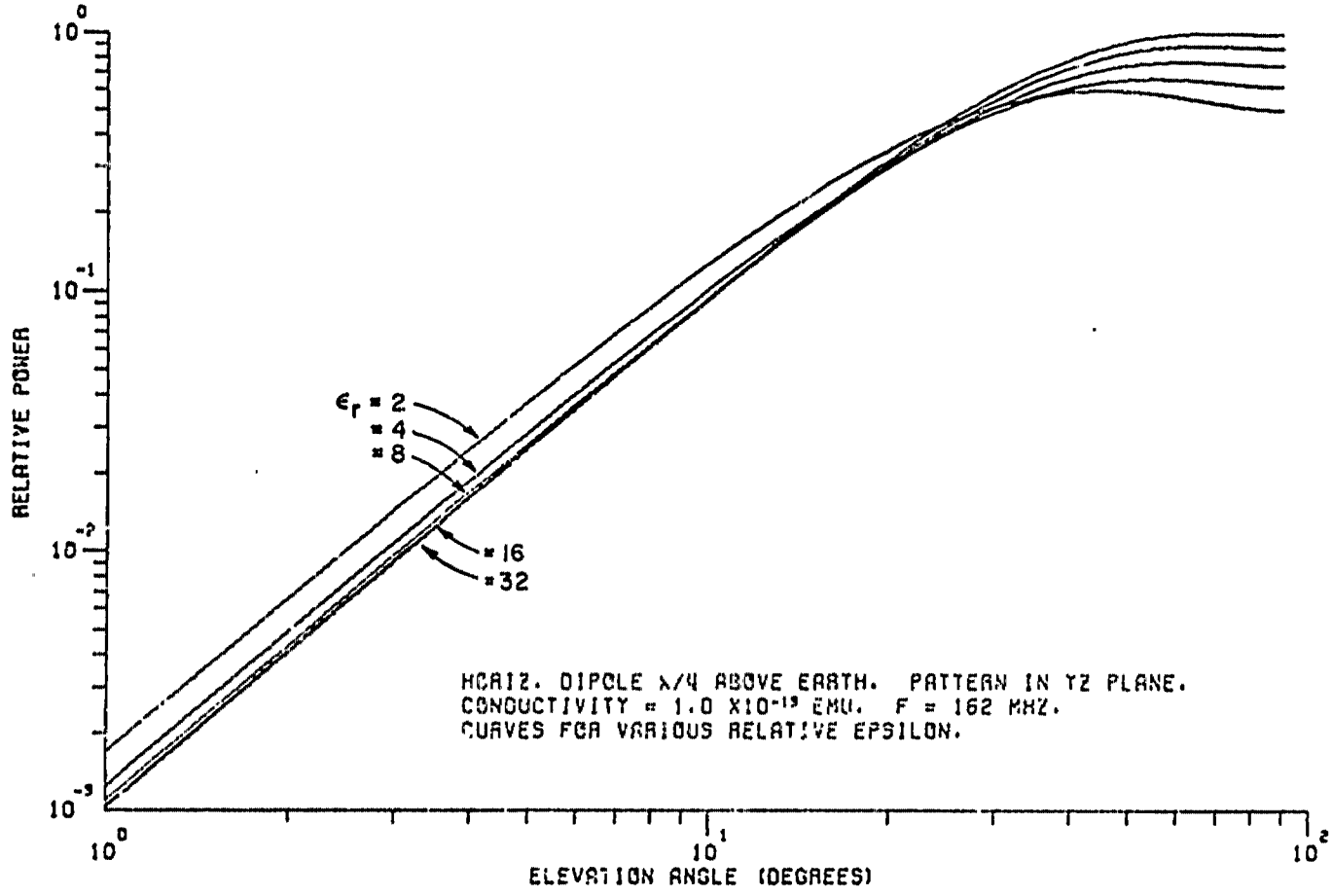

Fig. 21. Patterns for horizontal dipole in the yz plane with $\sigma=10^{-13}$ emu versus ϵ_r.

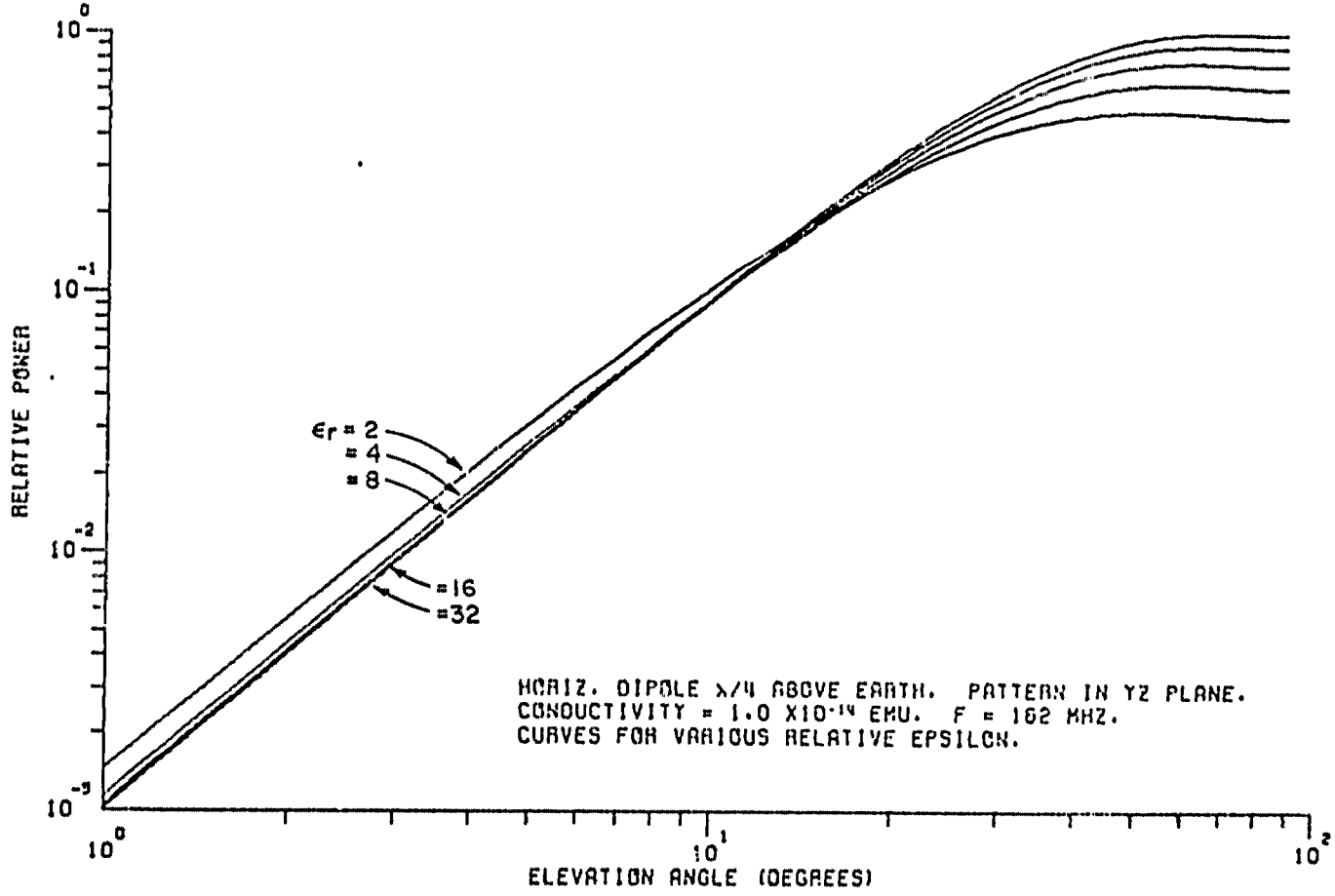

Fig. 22. Patterns for horizontal dipole in the yz plane with $\sigma = 10^{-14}$ emu versus ϵ_r.

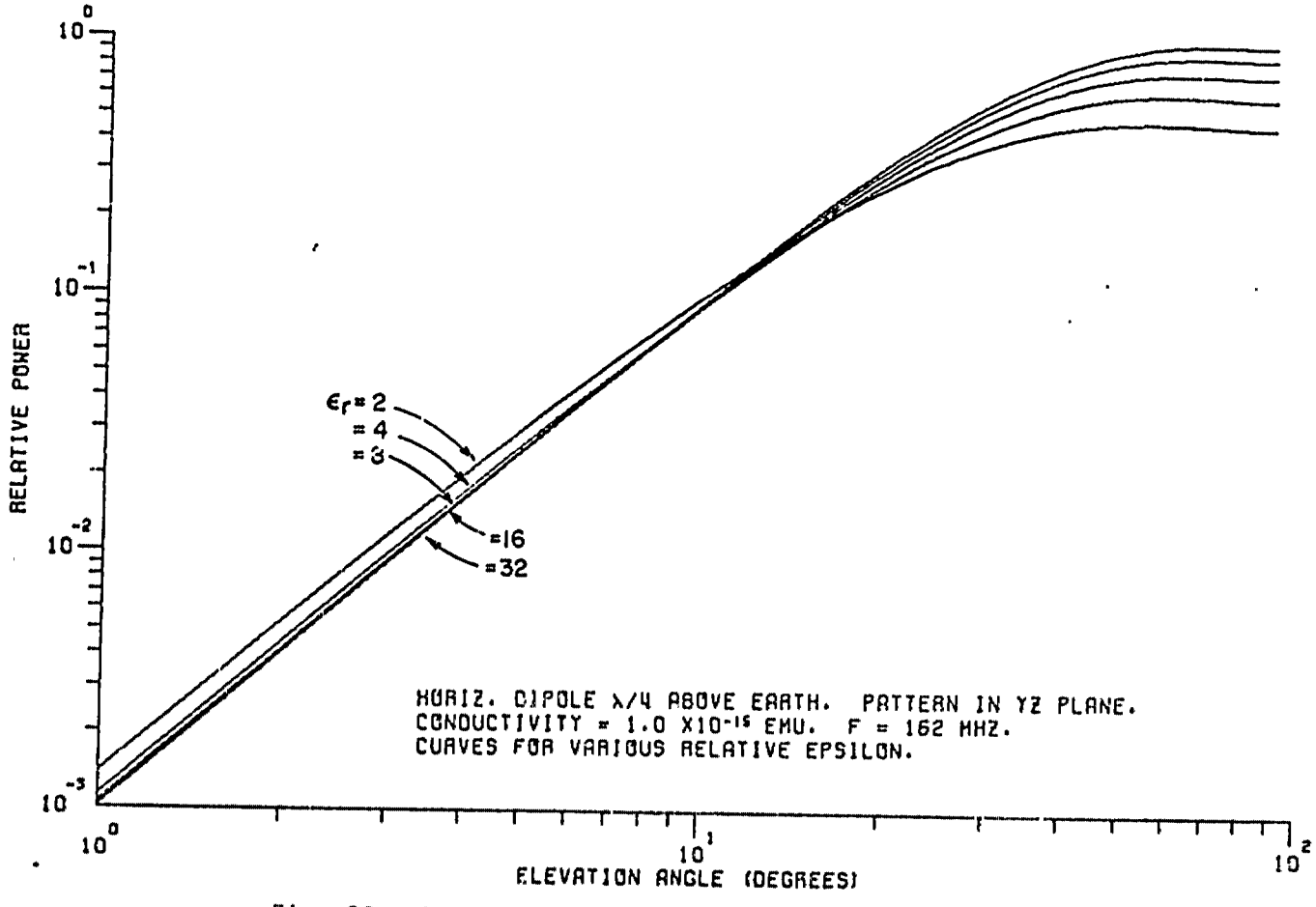

Fig. 23. Patterns for horizontal dipole in the yz plane with $\sigma=10^{-15}$ emu versus ϵ_r.

where,

$$(28)\qquad \vec{A} = \hat{i}\hat{r}\,E'^{h}_{r}\cos\phi + \hat{i}\hat{\phi}E'^{h}_{\phi}\sin\phi + \hat{i}\hat{k}E'^{h}_{z}\cos\phi$$
$$+ \hat{j}\hat{r}E'^{h}_{r}\sin\phi - \hat{j}\hat{\phi}E'^{h}_{\phi}\cos\phi + \hat{j}\hat{k}E'^{h}_{z}\sin\phi$$
$$+ \hat{k}\hat{r}E^{v}_{r} \qquad + 0 \qquad + \hat{k}\hat{k}E^{v}_{z}.$$

Note that the $\hat{j}\hat{\phi}$ term of $\vec{A}$ differs in sign from that given by Norton[10], and it is felt that this is probably a typographical error in Norton's paper.

The unprimed electric field components are defined in Eqs. (8) and (10)-(14), and the primed components are related to the unprimed components by

$$(29a)\qquad E^{h}_{r} = E'^{h}_{r}\cos\phi$$

$$(29b)\qquad E^{h}_{\phi} = E'^{h}_{\phi}\sin\phi$$

$$(29c)\qquad E^{h}_{z} = E'^{h}_{z}\cos\phi\ .$$

θ and ϕ are defined in Fig. 2 and are in general functions of $(\vec{R}-\vec{R}')$. Comparing Eqs. (10)-(14) and (28), (29) we see that all field components in Eq. (28) can be evaluated without dividing by $\sin\phi$ or $\cos\phi$.

It seems reasonable that the fields radiated by $I(\vec{R}')$ would be closely approximated by the fields radiated by several infinitesimal current elements orientated collinear with and located along the wire, and having a complex magnitude related to the complex magnitude of $I(\vec{R}')$ at their locations. To make this more clear consider for example a vertical linear antenna of length L located along the z axis as shown in Fig. 24b. In this case Eq. (27) becomes

$$(30)\qquad \vec{E}(\vec{R}) = \int_{z'_a}^{z'_b} I(z')\cdot\vec{A}(\vec{R}-\vec{z}')dz'.$$

Our approach will be to numerically evaluate the integral of Eq. (30). For example we could use the trapezoidal rule which is the approximation

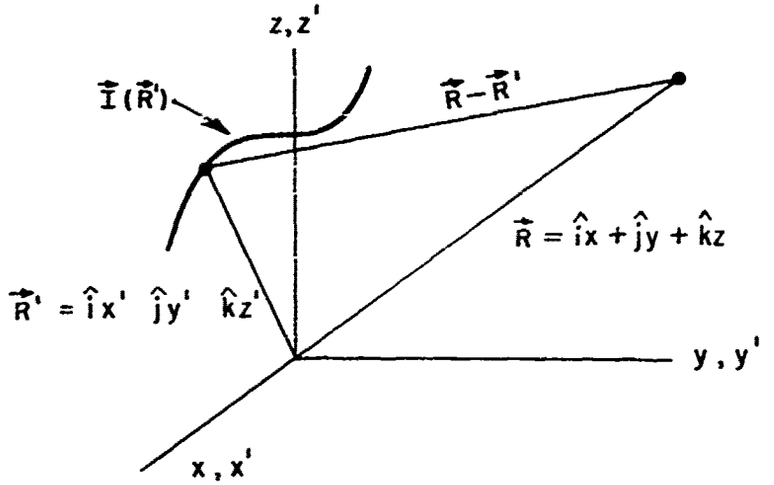

(a)

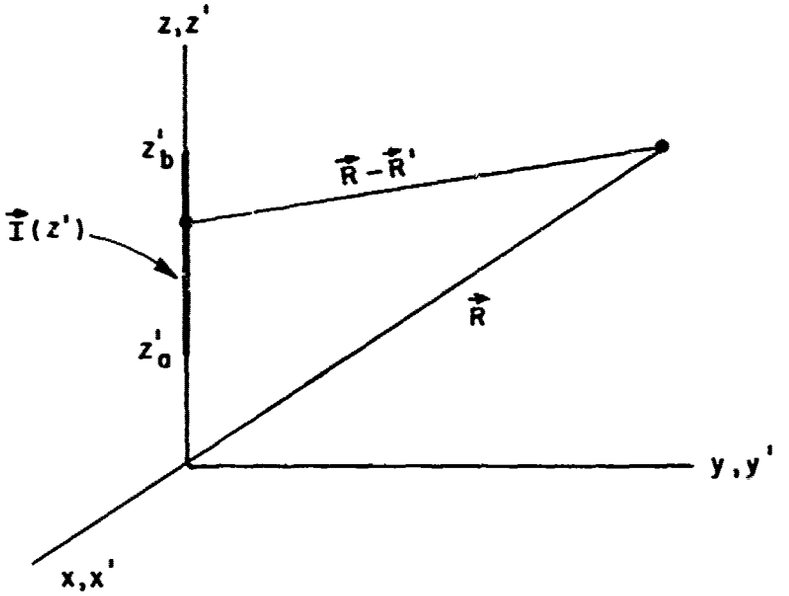

(b)

Fig. 24. Current distributions on a wire (a) Arbitrary wire, (b) Straight wire aligned with the z axis.

$$(31)\qquad \int_{x_1}^{x_2} f(x)dx \approx \frac{x_2-x_1}{2}[f(x_1)+f(x_2)].$$

In this case Eq. (30) becomes

$$(32)\qquad \vec{E}(\vec{R}) \approx \frac{L}{2}[\vec{F}(z'_a)+\vec{F}(z'_b)]$$

where

$$\vec{F}(z')=\vec{I}(z')\cdot\vec{\vec{A}}(\vec{R}-\vec{z}').$$

In essence we are approximating the continuous current distribution of Fig. 23b by two infinitesimal current elements located at z'_a and z'_b and of magnitude and orientation given by $\frac{L}{2}\vec{I}(z'_a)$ and $\frac{L}{2}\vec{I}(z'_b)$ respectively. If there is considerable variation of the current over the length of the wire we may wish to split the integral of Eq. (30) into two parts to get

$$(33)\qquad \vec{E}(\vec{R}) \approx \frac{L}{4}\left[\vec{F}(z'_a)+\vec{F}\left(\frac{z'_a+z'_b}{2}\right)\right] + \frac{L}{4}\left[\vec{F}\left(\frac{z'_a+z'_b}{2}\right)+\vec{F}(z'_b)\right]$$

$$\approx \frac{L}{2}\left[\frac{1}{2}\vec{F}(z'_a)+\vec{F}\left(\frac{z'_a+z'_b}{2}\right)+\frac{1}{2}\vec{F}(z'_b)\right] .$$

Clearly we could continue this splitting to obtain

$$(34)\qquad \vec{E}(\vec{R}) \approx \Delta L\left[\frac{1}{2}\vec{F}(z'_0)+\vec{F}(z'_1)+\cdots+\vec{F}(z'_{N-1})+\frac{1}{2}\vec{F}(z'_N)\right]$$

where,

$$(35a)\qquad \Delta L = (z'_b-z'_a)/N$$

$$(35b)\qquad z'_n = z'_a + \frac{n}{N}L \qquad n=0,1,2,\cdots N.$$

Inspection of Eq. (34) shows that we are representing the continuous current distribution by N+1 infinitesimal current elements located at z'_n and with complex magnitude and orientation

$\frac{\Delta L}{2}\, I(z_n')$ n=0 or N

$\Delta L\, I(z_n')$ otherwise.

Any numerical integration, such as Gaussian quadrature or Simpson's rule, will permit representing a continuous distribution by a series of infinitesimal current elements whose location, orientation, and magnitude are most obvious after the numerical integration is written out explicitly.

While in this example we chose our current distribution to be aligned with the z-axis, this in no way restricts our procedure. For example if we wish to approximate the fields radiated by the current distribution in Fig. 25 by one application of the trapezoidal rule, we would have

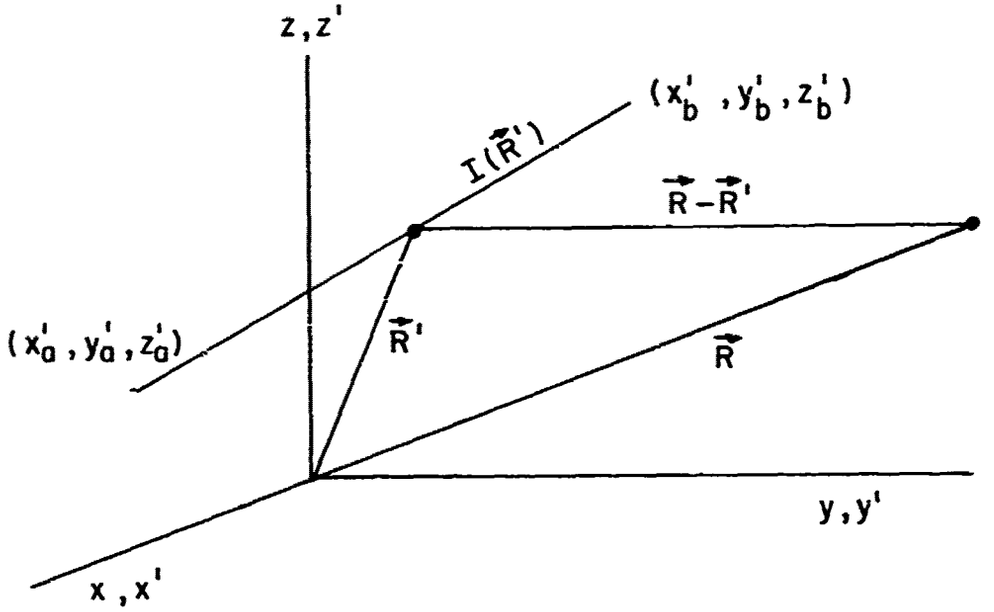

Fig. 25. Current distribution on an arbitrarily orientated straight wire.

$$(36)\qquad \vec{E}(\vec{R}) = \int_{\text{wire}} \vec{I}(\vec{R}') \cdot \vec{\vec{A}}(\vec{R}-\vec{R}')\, d\ell \approx \frac{\Delta L}{2}\left[\vec{F}(x_a', y_a', z_a') + \vec{F}(x_b', y_b', z_b')\right]$$

where $\Delta L = \sqrt{(x_a'-x_b')^2+(y_a'-y_b')^2+(z_a'-z_b')^2}$.

A large class of antennas can be modeled by a wire-grid consisting of many straight wire segments. Often several segments connect at one point. In representing such a complex structure by a finite number of infinitesimal electric current elements, the path of integration in Eq. (27) is over the entire wire-grid structure. To avoid errors, it is recommended that this integral be split into smaller parts to avoid integrating past a point where two or more wires connect.

Far-field patterns calculated using the methods of this report are compared with patterns found in the literature in Appendix II.

Thus far we have treated only current distributions as would exist on a wire antenna, or if a wire-grid model was made of a complex antenna. The technique can however be extended to two or three dimensional sources. The approach would be to numerically evaluate the surface or volume integral corresponding to Eq. (27). This would replace the surface or volume integral by a double or a triple summation, the inspection of which would indicate the location and magnitude of the infinitesimal electric current elements.

We will now summarize the ideas of the preceding sections. The problem we wish to solve is that of finding the pattern of an antenna in the vicinity of a flat finitely conducting earth. We use the approximation that the current on the antenna is unaffected by the presence of the earth, and thus, may be calculated assuming the antenna to be in free space. This is a reasonable approximation if the antenna is shielded from the earth by, for example, a small perfectly conducting ground plane or is sufficiently elevated above the earth. Next the continuous currents on the wires of the antenna are represented by a number of infinitesimal current elements. The fields of the individual elements can be found using Eqs. (8) and (10)-(14), and then summed to yield the antenna pattern. This procedure will be applied to several antennas in the next section.

V. THEORETICAL ANTENNA PATTERNS

We now wish to apply the methods of Sections II and IV to determine the far field patterns of four antennas of particular interest:

1. A quarter wave monopole over four quarter wave arms as shown in Fig. 26.

2. A 3-1/2 turn multiturn loop (MTL) as shown in Fig. 27.

3. A 12 turn "picket fence" MTL as shown in Fig. 28.

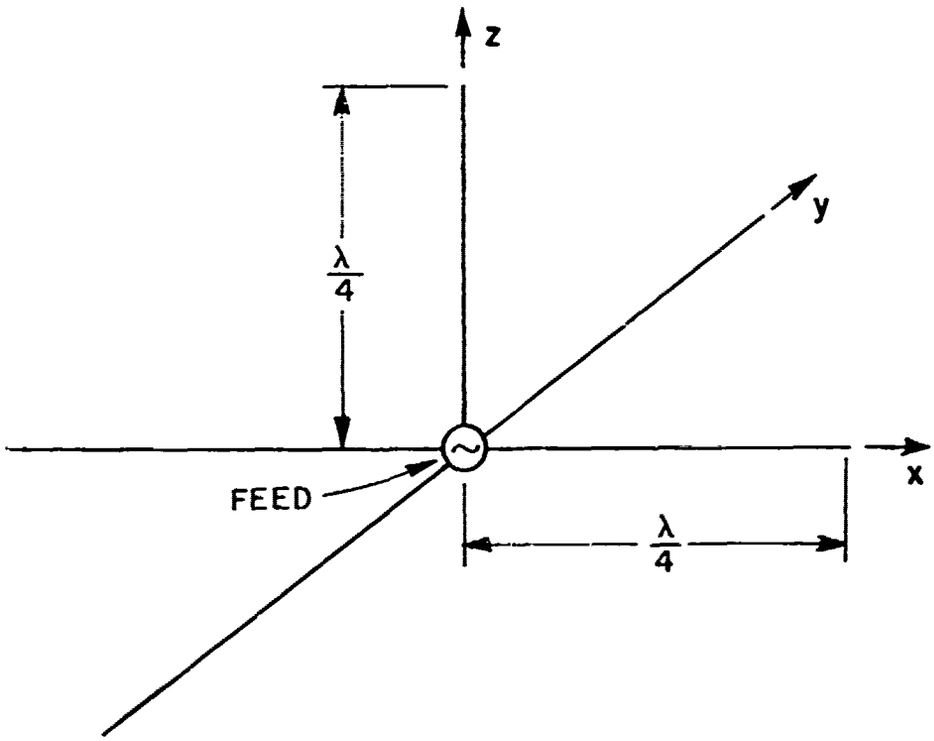

Fig 26. Antenna 1 - A quarter wave monopole over four quarter wave arms.

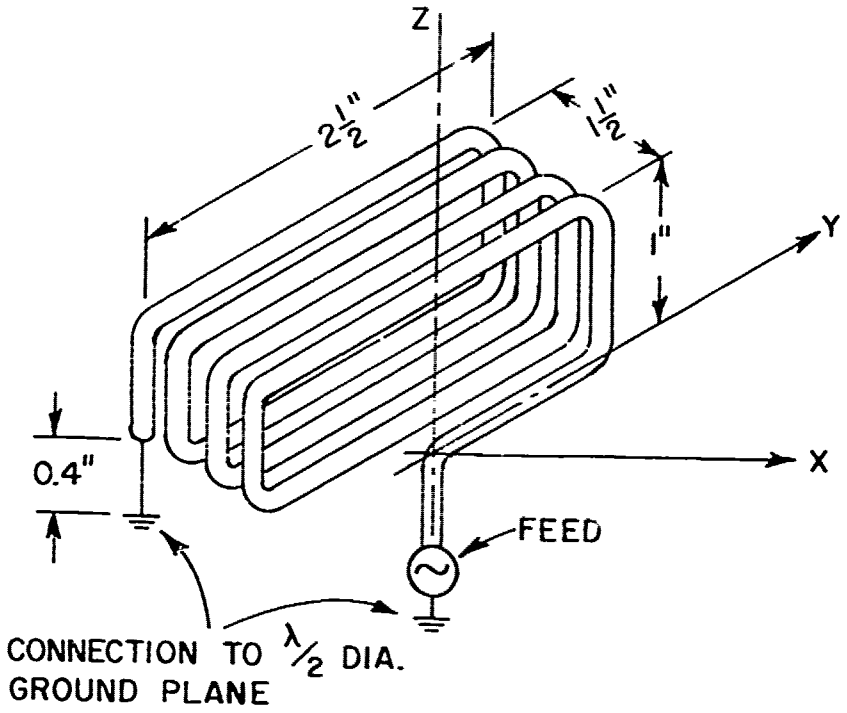

Fig 27. Antenna 2 - 3-1/2 turn MTL.

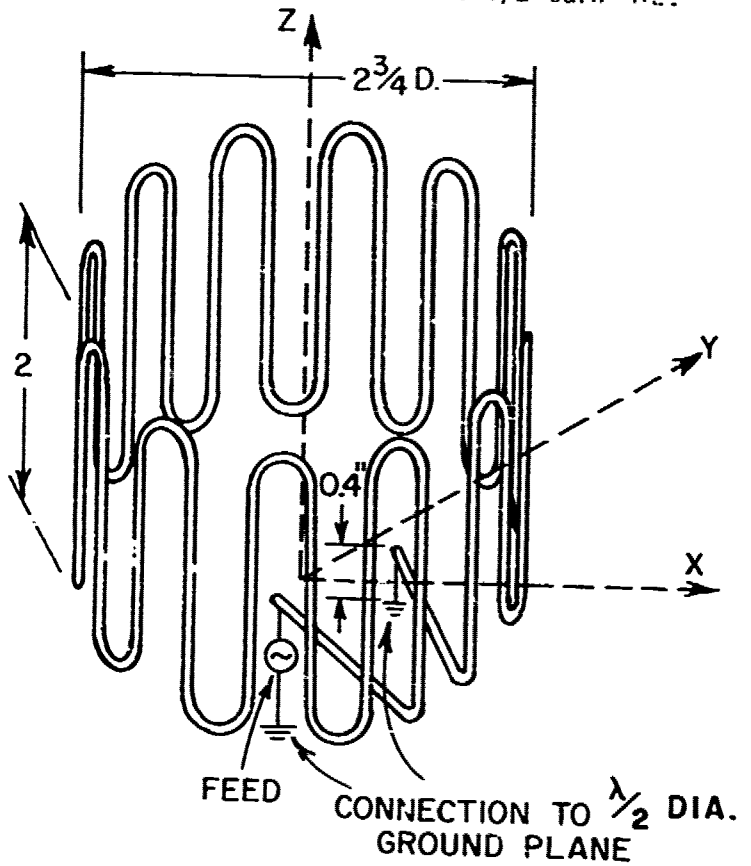

Fig. 28. Antenna 3 - 12 turn "picket fence" MTL.

4. A 12 turn "picket fence" MTL as shown in Fig. 28, but with a four inch diameter reflecting plate placed 0.4" above the MTL.

Antennas 2, 3, and 4 are placed over a perfectly conducting ground plane $\lambda/2$ in diameter. The four horizontal quarter wave arms of antenna 1 approximate a ground plane $\lambda/2$ in diameter. The small perfectly conducting ground plane is then placed $\lambda/8$ over a lossy earth with $\epsilon_r = 5$ and $\sigma = 3.0 \times 10^{-13}$ emu = 0.03 mho/meter, as shown in Fig. 29a. Antenna power patterns will be shown for R = 1 km, f = 162 MHz, and for various antenna tilt angles as defined in Fig. 29b. For large tilt angles the $\lambda/2$ diameter ground plane intersects the lossy earth. This, a problem since subroutine DIPOLE, used in making the calculations in this section, applies only to sources located above the lossy earth. However, since we are mainly interested in seeing trends as the antenna is tilted, this problem is avoided by simply ignoring the few sources which are located beneath the earth's surface.

As has been pointed out, a calculation of the far-field pattern of any antenna begins with a calculation or an approximation of the currents flowing on the antenna. Thus, for antennas 2-4, we begin by making a wire-grid model of the MTL antenna, the $\lambda/2$ diameter ground plane, and for antenna 4 the 4 inch reflecting plate. Antenna 1 is identical to its wire-grid model. Next the currents flowing on the antenna are calculated using a moment method solution, and the assumption that the wire-grid model is located in free space. As indicated in Section IV the currents flowing on the wire-grid model are replaced by a number of infinitesimal electric current elements. Finally, the fields of these infinitesimal sources are calculated using Eqs. (8), (10)-(14), and (27), (28) and added vectorially to form the antenna field patterns. Power patterns are obtained from the field patterns by taking the magnitude squared of the field and multiplying by the antenna efficiency defined as

$$(37) \qquad \text{Efficiency} = \frac{P_{in} - P_{loss}}{P_{in}} = \frac{P_{rad}}{P_{in}}$$

where P_{in}, P_{loss}, P_{rad} are power input, ohmic power losses, and the radiated power respectively. The efficiencies were measured[12] using a method employed by Wheeler[13]. The efficiency of a MTL is strongly dependent upon the volume it occupies, on its geometry, and on the conductor resistance and therefore the diameter of the wire being used. A study is presently being conducted at the Electro-Science Laboratory to optimize the efficiency of MTL antennas. At this point typical results are 35% for antenna 2, and 20% for antennas 3 or 4. However, these values are not to be taken as being the best possible for a given MTL, but simply typical results to date. For comparison, the efficiency of antenna 1 is taken to be 70%.

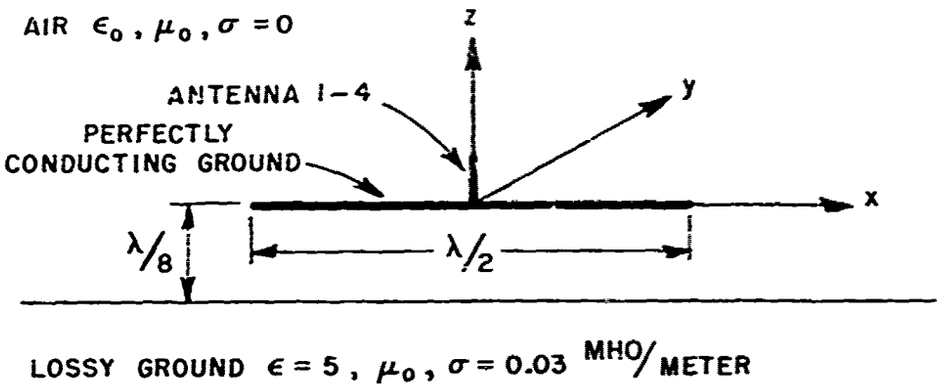

(a)

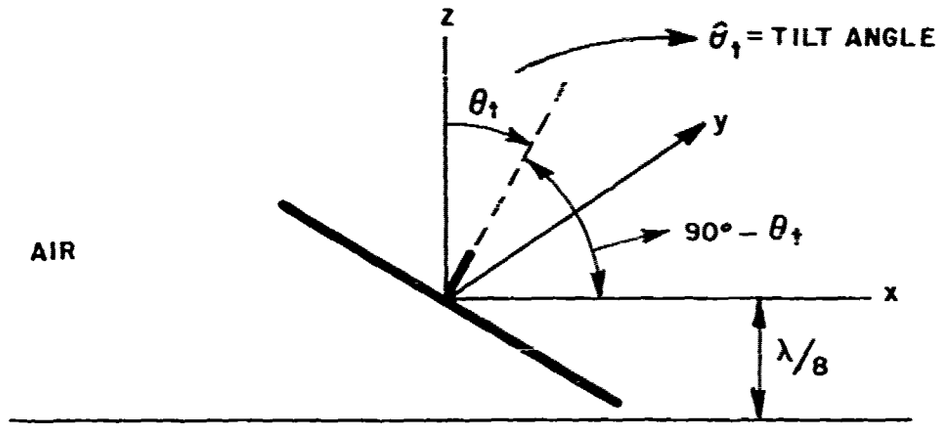

(b)

Fig. 29. (a) Geometry of antennas with respect to the lossy ground, (b) Geometry for antenna tilt angle.

Patterns will be shown for the antennas tilted through some angle θ_t as shown in Fig. 29b. Note that the antennas are assumed to be tilted directly toward the positive x axis. When an antenna is tilted through some angle θ_t the location and orientation of the infinitesimal sources representing the antenna are changed, but not their magnitude or phase. This is a result of calculating the antenna currents assuming the antenna to be in free space. Clearly as θ_t increases the $\lambda/2$ ground plane becomes less effective in shielding the antenna from the lossy earth, and our "free space assumption" becomes less valid.

In Figs. 30-33 the far-field power patterns for antennas 1-4 are shown. Patterns are shown for $\theta_t = 0°$, 30°, and 60°, and in both the xz and yz planes. The patterns are normalized so that the power into each antenna is one watt, and so that the peak power radiated by antenna 1 corresponds to 0 db.

At low elevation angles and $\theta_t = 0°$ the 3-1/2 turn MTL (antenna 2) is several dB below the $\lambda/4$ monopole over four $\lambda/4$ arms (antenna 1). However, when $\theta_t = 60°$ and for low elevation angles near the positive x axis antenna 2 is several dB superior to antenna 1. In Figs. 32 and 33 the 12 turn picket fence MTL is seen to have a very unsymmetrical pattern in the xz plane. This is largely due to the antenna being fed unsymmetrically. If a symmetric pattern is desired, a symmetric feed is required. Comparing Figs. 32 and 33 we see that the 4 inch plate above the MTL has almost no effect on the far-field pattern. Antennas 3 and 4 exhibit behavior similar to antenna 2 in that, at low elevation angles and $\theta_t = 0°$ antenna 1 is several dB superior, while at larger θ_t the 12 turn picket fence MTL may be superior. MTL antennas have been investigated experimentally, and were found to have patterns superior to the quarter wave monopole over four quarter wave arms at low elevation angles for the case $\theta_t = 60°$. These measurements will be presented in a future report.

It is possible to convert the relative power in dB values from Figs. 30-33 directly to the absolute magnitude of the field strength in volts/meter. This can be done via the relationship

$$|E| = (2.25 \times 10^{-4}) \cdot 10^{P/20} \text{ volts/meter.} \tag{38}$$

Here P is a relative power value taken from Figs. 30-33 and will be less than or equal to zero. Equation (38) assumes 1 watt of real power input to the antenna.

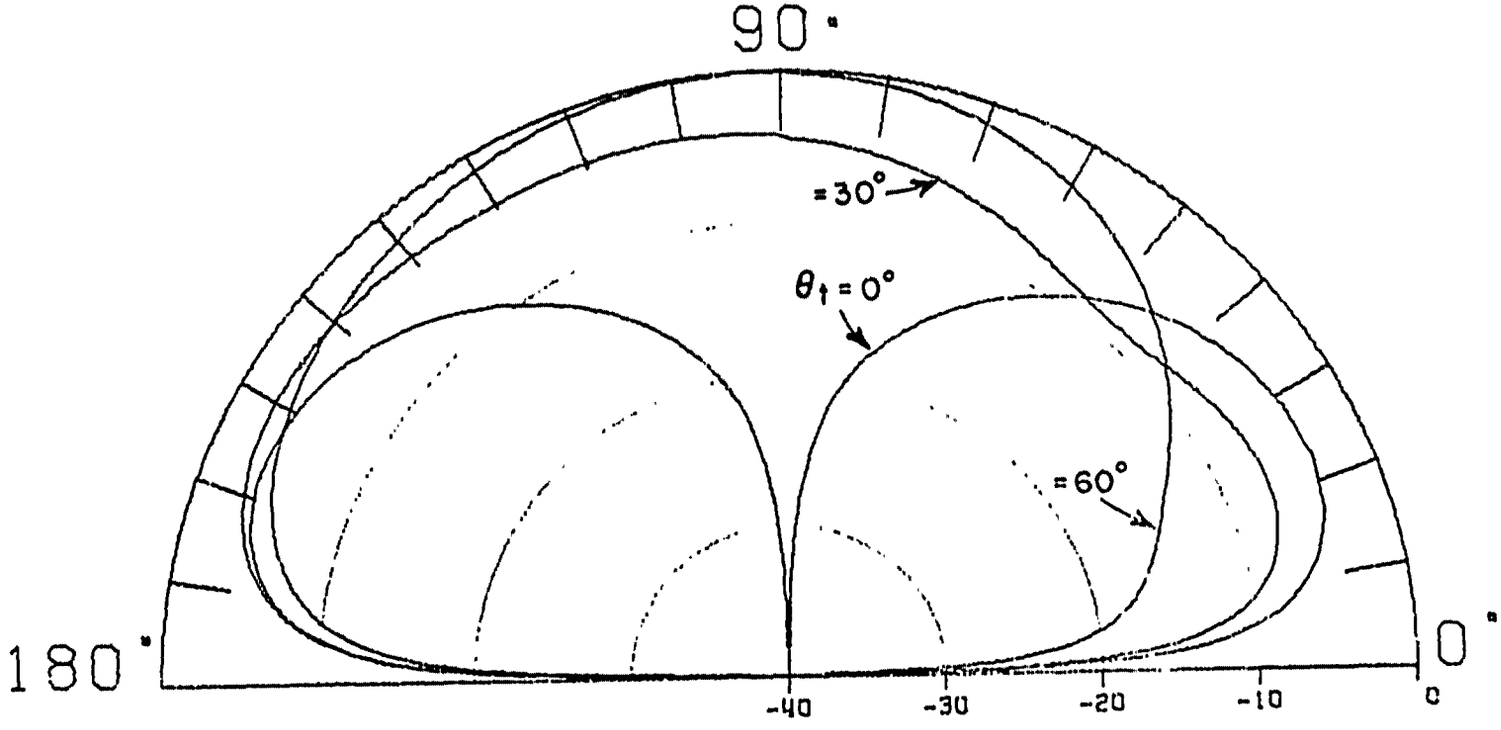

λ/4 DIPOLE OVER FOUR λ/4 ARMS.
CONDUCTIVITY = 0.03 MHO/METER. F = 162 MHZ.
RELATIVE EPSILON =.5.
RELATIVE POWER PATTERNS IN THE XZ PLANE.
CURVES FOR VARIOUS TILT ANGLES.

Fig. 30. Power patterns for antenna 1 versus tilt angle
(a) Pattern in the xz plane.

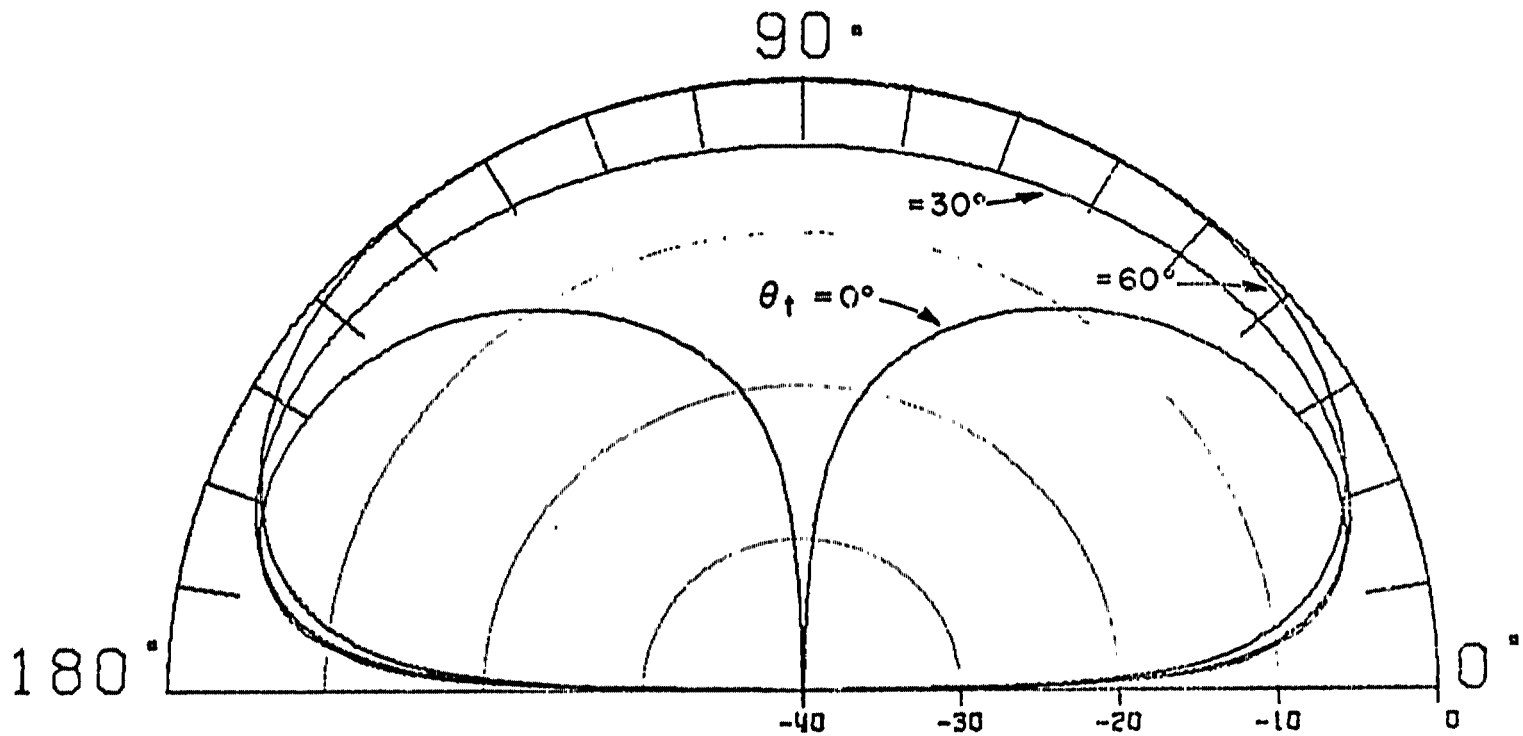

λ/4 DIPOLE OVER FOUR λ/4 ARMS.
CONDUCTIVITY = 0.03 MHO/METER. F = 162 MHZ.
RELATIVE EPSILON = 5.
RELATIVE POWER PATTERNS IN THE YZ PLANE.
CURVES FOR VARIOUS TILT ANGLES.

Fig. 30. Power patterns for antenna 1 versus tilt angle
(b) Pattern in the yz plane.

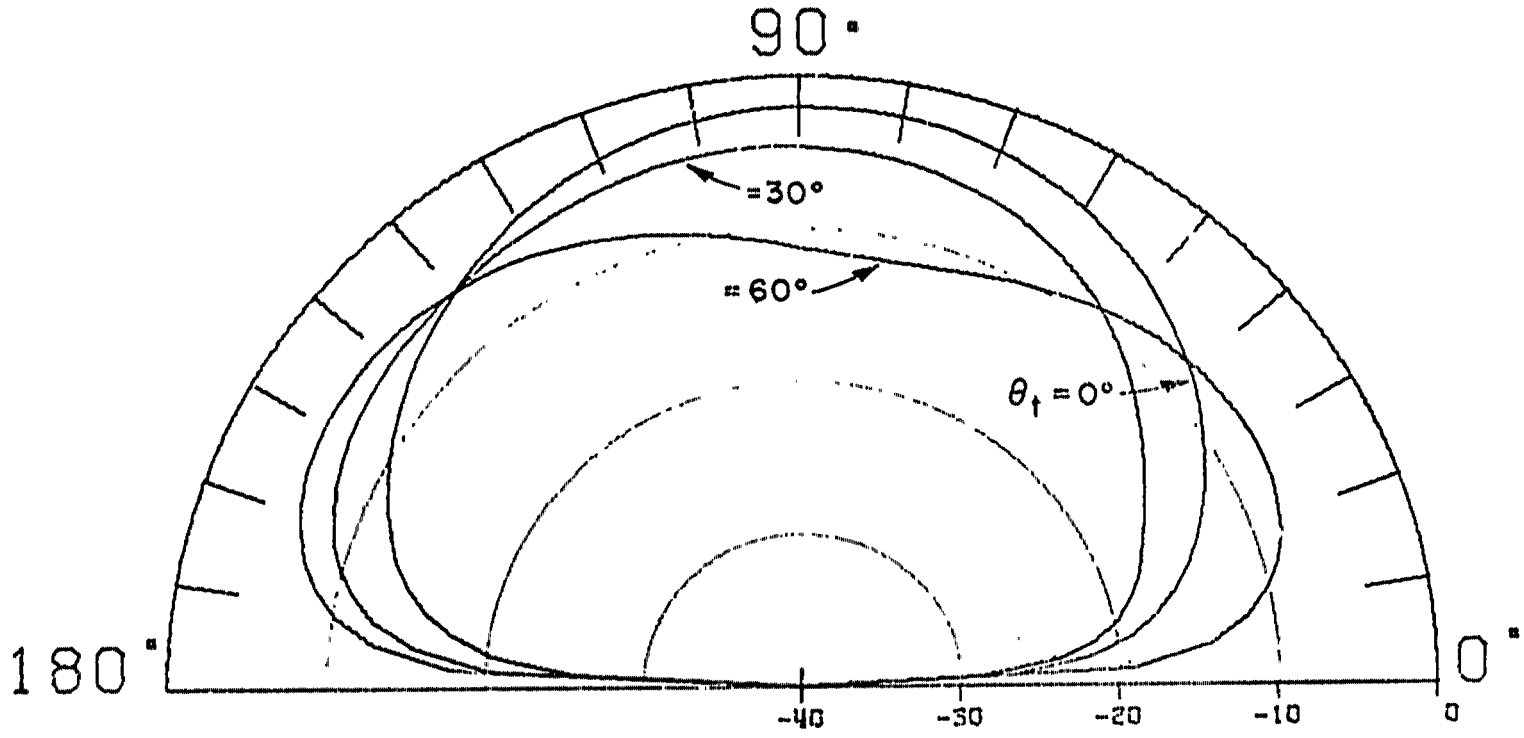

3 AND 1/2 TURN MTL OVER A λ/2 GROUND PLANE.
CONDUCTIVITY = 0.03 MHO/METER. F = 162 MHZ.
RELATIVE EPSILON = 5.
RELATIVE POWER PATTERNS IN THE XZ PLANE.
CURVES FOR VARIOUS TILT ANGLES.

Fig. 31. Power patterns for antenna 2 versus tilt angle
(a) Pattern in the xz plane.

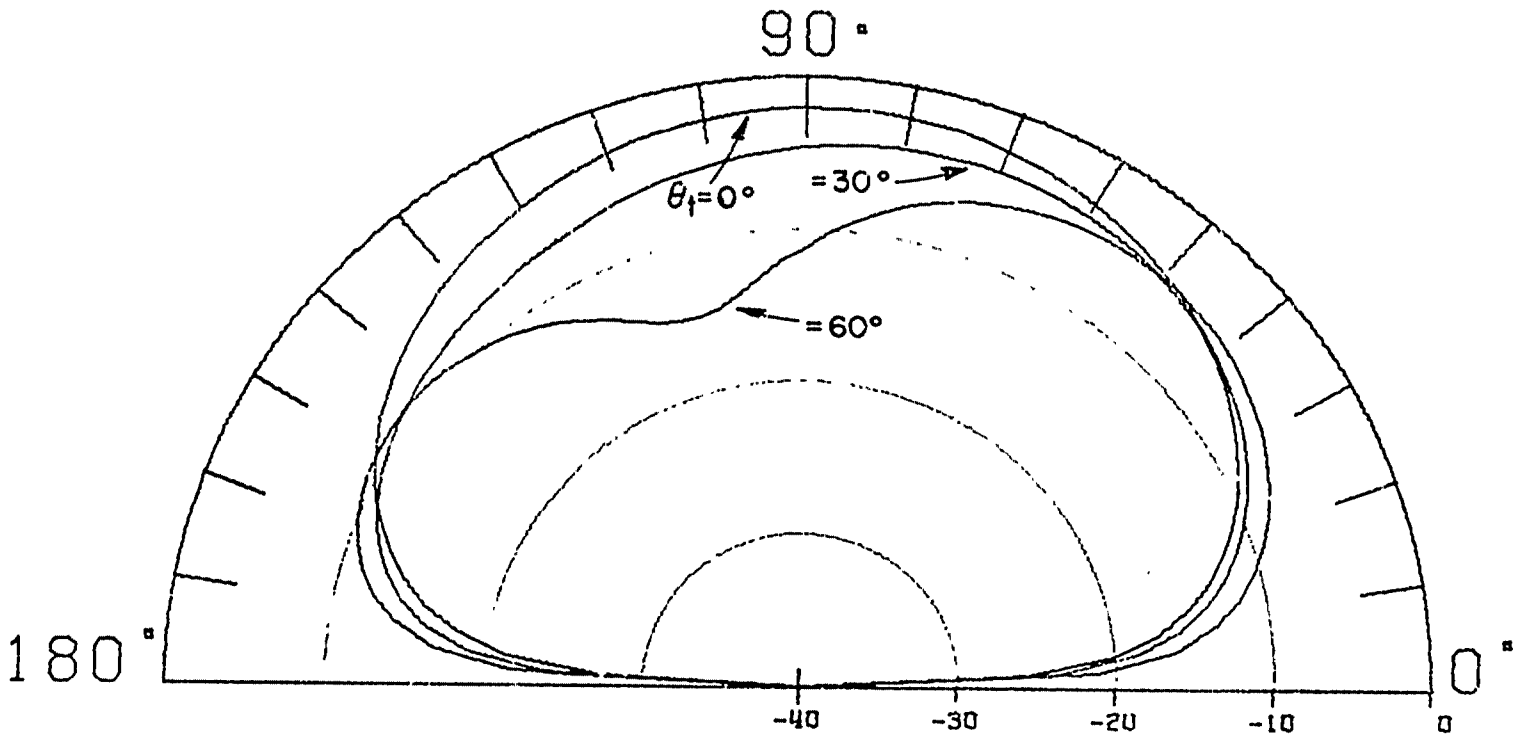

3 AND 1/2 TURN MTL OVER A λ/2 GROUND PLANE.
CONDUCTIVITY = 0.03 MHO/METER. F = 162 MHZ.
RELATIVE EPSILON = 5.
RELATIVE POWER PATTERNS IN THE YZ PLANE.
CURVES FOR VARIOUS TILT ANGLES.

Fig. 31. Power Patterns for antenna 2 versus tilt angle
(b) Pattern in the yz plane.

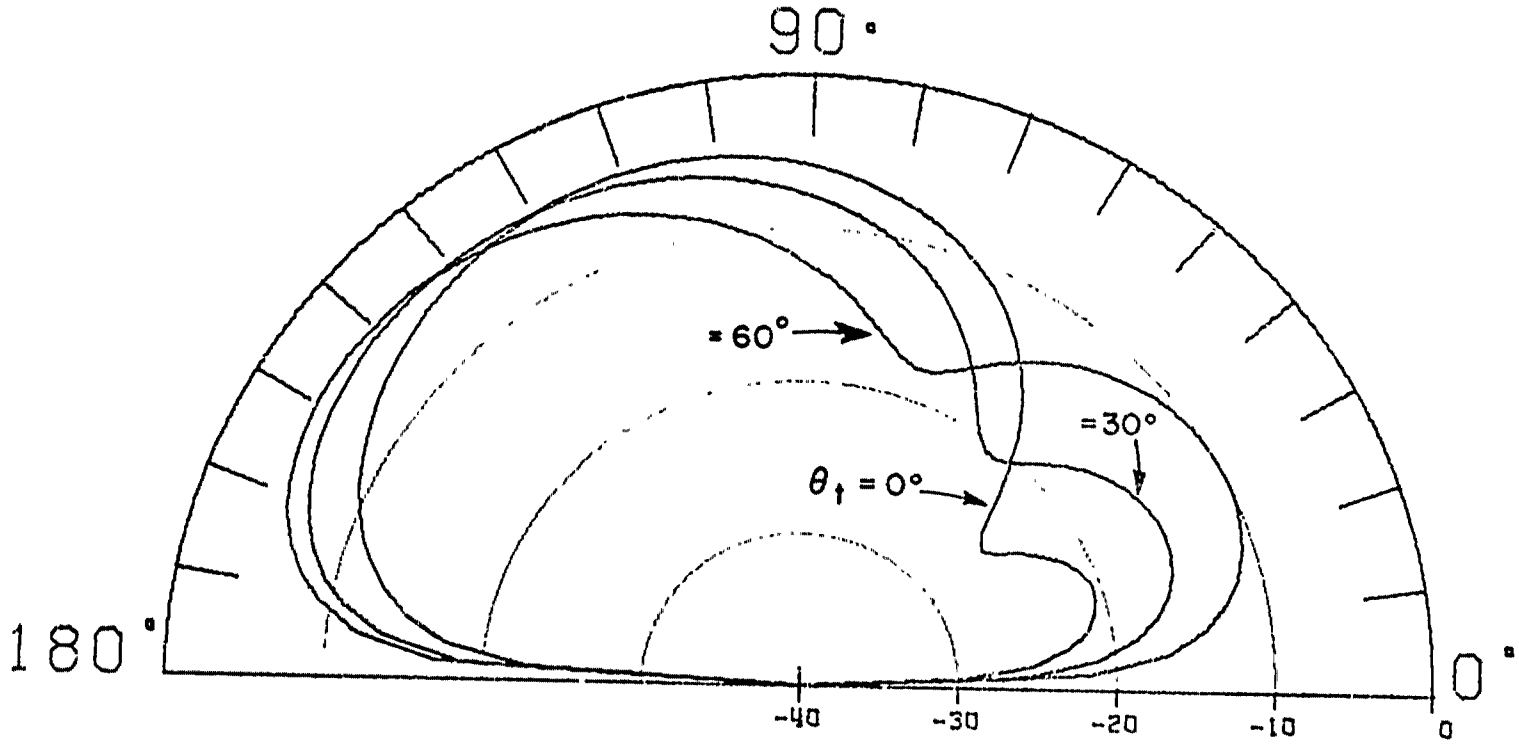

12 TURN PICKET FENCE MTL OVER A λ/2 GROUND PLANE.
CONDUCTIVITY = 0.03 MHO/METER. F = 162 MHZ.
RELATIVE EPSILON = 5.
RELATIVE POWER PATTERNS IN THE XZ PLANE.
CURVES FOR VARIOUS TILT ANGLES.

Fig. 32. Power patterns for antenna 3 versus tilt angle
(a) Pattern in the xz plane.

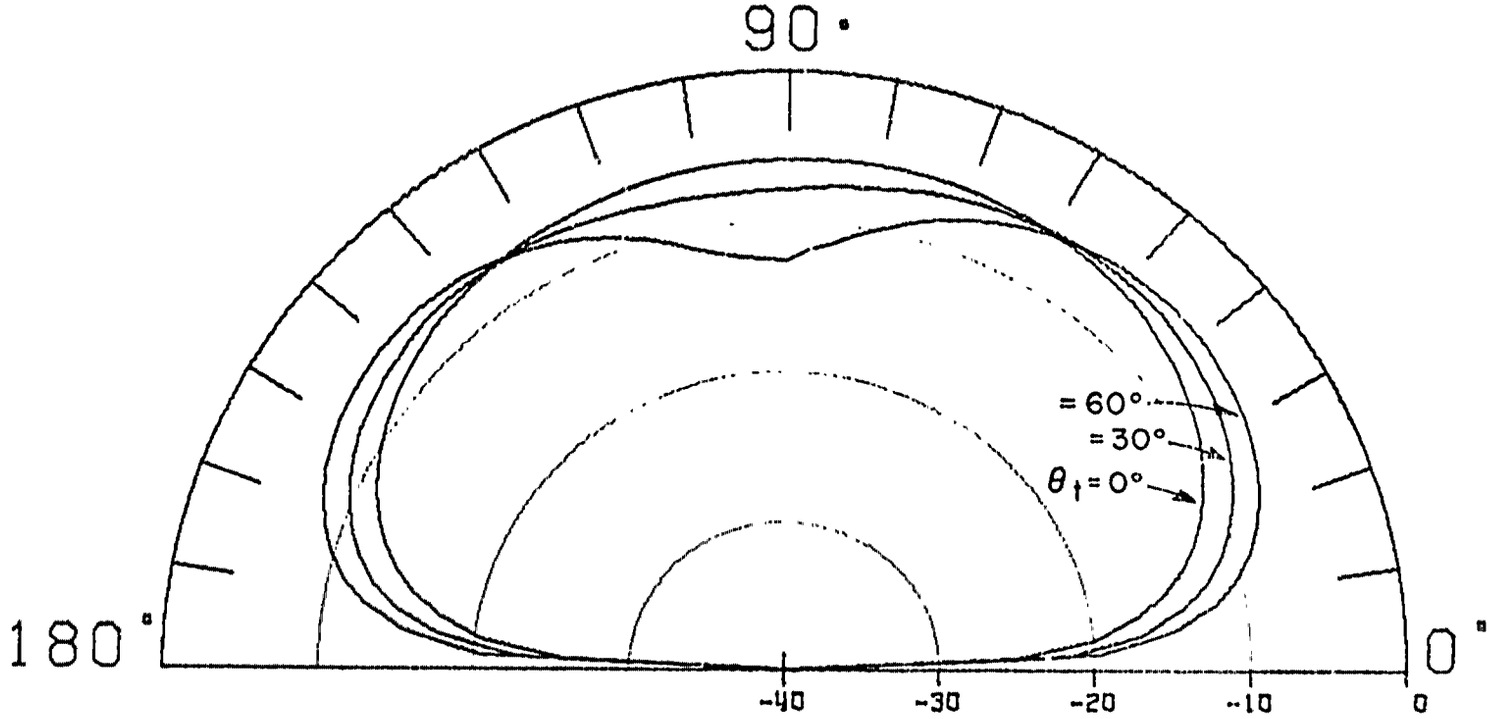

12 TURN PICKET FENCE MTL OVER A λ/2 GROUND PLANE.
CONDUCTIVITY = 0.03 MHO/METER. F = 162 MHZ.
RELATIVE EPSILON = 5.
RELATIVE POWER PATTERNS IN THE YZ PLANE.
CURVES FOR VARIOUS TILT ANGLES.

Fig. 32. Power patterns for antenna 3 versus tilt angle (b) Pattern in the yz plane.

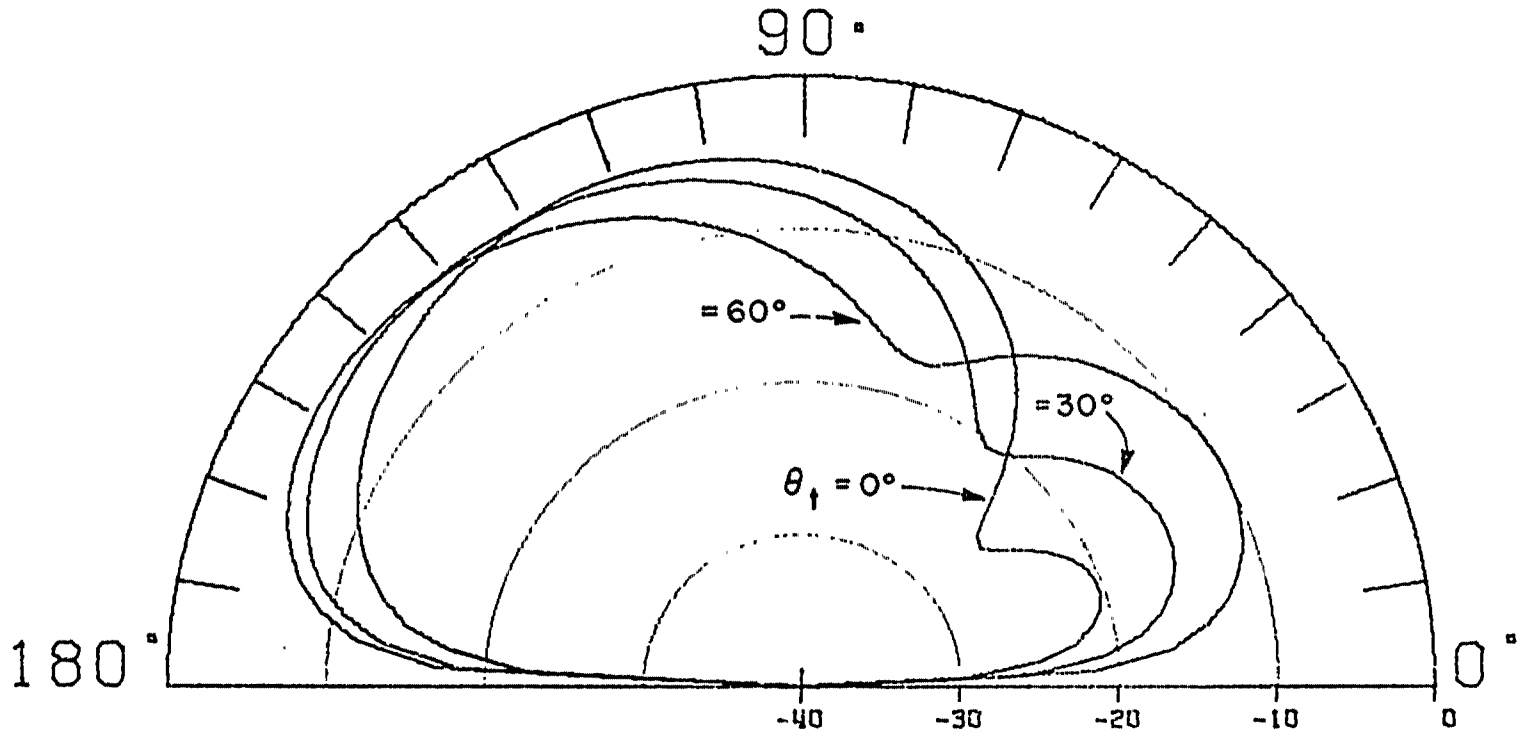

12 TURN PICKET FENCE MTL OVER A λ/2 GROUND PLANE.
4 INCH DIA. REFLECTING PLATE LOCATED ABOVE THE MTL.
CONDUCTIVITY = 0.03 MHO/METER. F = 162 MHZ.
RELATIVE EPSILON = 5.
RELATIVE POWER PATTERNS IN THE XZ PLANE.
CURVES FOR VARIOUS TILT ANGLES.

Fig. 33. Power patterns for antenna 3 versus tilt angle
(a) Pattern in the xz plane.

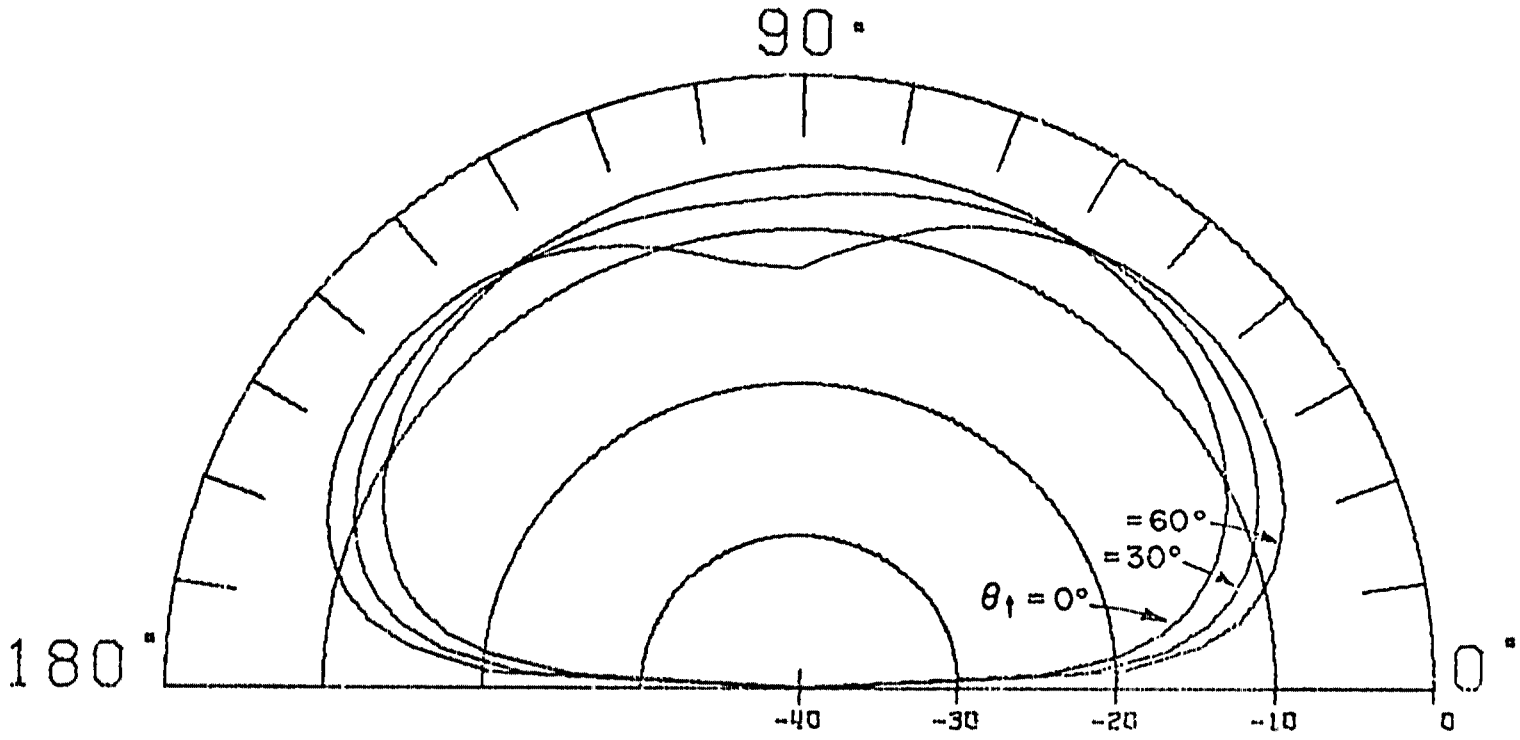

12 TURN PICKET FENCE MTL OVER A λ/2 GROUND PLANE.
4 INCH DIA. REFLECTING PLATE LOCATED ABOVE THE MTL.
CONDUCTIVITY = 0.03 MHO/METER. F = 162 MHZ.
RELATIVE EPSILON = 5.
RELATIVE POWER PATTERNS IN THE YZ PLANE.
CURVES FOR VARIOUS TILT ANGLES.

Fig. 33. Power patterns for antenna 3 versus tilt angle
(b) Pattern in the yz plane.

VI. SUMMARY AND CONCLUSIONS

In this report we have had two basic aims directed toward accomplishing the objective of this investigation as stated in Section I. These aims will be summarized in this section. The first aim was to obtain a qualitative indication as to how the presence of a lossy earth affects the far-field VHF power pattern of an antenna located in air above the lossy earth. Our second aim was to describe a computationally straightforward method for determining the far-field pattern of an antenna located in air near a lossy earth.

To obtain a qualitative indication of the lossy earth's effect it was decided to study in detail the infinitesimal horizontal and vertical electric current elements instead of specializing to a specific antenna geometry. First, computationally useful expressions for the fields radiated by the current elements were presented and it was shown how these expressions could be interpreted in terms of space waves and surface waves.

Space wave fields have their maximum radiation away from the earth's surface, are characterized by a $1/R$ radial dependence in the far-field, and vanish at the earth's surface. Surface waves have their maximum radiation at the earth's surface, and are characterized by a $1/R^2$ radial dependence in the far-field for frequencies above approximately 100 MHz and typical ground constants. Thus, the surface wave is only important at very low elevation angles.

Far-field power patterns are shown for horizontal and vertical elements located between 0 and 2λ from the earth's surface. It was found, as expected, that vertical elements are better radiators at low elevation angles, while horizontal elements are better radiators at large elevation angles. Elevating an element from the earth's surface was found to generally increase the radiation at low elevation angles.

Far-field power patterns were also shown for the horizontal and vertical element located $\lambda/4$ above the earth and for varying ground parameters. It was found that near 200 MHz varying the ground conductivity from 0.1 to 0.0001 mho/meter has little effect on the element patterns. However, varying the relative permittivity from 2 to 32 increases the radiation at low elevation angles for vertical elements, but decreases it for horizontal elements.

Because in the far-field the space wave field varies as $1/R$ and the surface wave field varies as $1/R^2$ some error will be introduced in extrapolating a pattern from one radial distance to another if the usual $1/R$ field dependence is assumed. At frequencies greater

than 160 MHz and typical ground constants it was found that extrapolating from R = 1 km to greater radial distances can be done with little error since the surface wave at these frequencies attenuates rapidly with distance from the source.

Determining the far-field pattern of an antenna can be thought of as consisting of two steps. First the current on the antenna must be determined. If the antenna is located near a lossy earth the exact solution will involve an integral equation which contains the Sommerfeld integral, and will be very difficult and time consuming to solve. Our approach was to assume that the antenna current was unchanged by the presence of the lossy earth, and thus it could be found using available computer programs for finding antenna currents in free space. This approximation is best applicable when the antenna is shielded from the lossy earth as by a cavity or a small perfectly conducting ground plane, or if the antenna is physically removed several wavelengths from the earth.

Regardless of how the antenna current was obtained the problem still remains to find the radiation pattern of a now known current distribution in the presence of the lossy earth. The exact solution involves an integration over the antenna. The integrand will contain the Sommerfeld integral and again will be difficult and time consuming to evaluate. Our approach was to replace the continuous current distribution on the antenna by a finite number of infinitesimal electric current elements. The fields of the individual elements can be evaluated using expressions developed by Norton[10], and then summed to yield the antenna pattern. The accuracy of this approach is discussed in Appendix II.

The above approximations were applied to calculate the far-field power patterns of several antennas located near a lossy earth. Specifically we compared the pattern of a quarter wave monopole above four quarter wave arms to the patterns of a few electrically small multiturn loop (MTL) antennas placed over a half wave diameter perfectly conducting ground plane.

None of the antennas considered had an overall superior far-field pattern. However, for large tilt angles (e.g., $\theta_t = 60°$) with the antenna tilting generally in the direction of the observer, the theoretical calculations tend to indicate a higher level of radiation at low elevation angles from the MTL than from the quarter-wave dipole (e.g., Fig. 31a and Fig. 30a respectively). This geometry was of particular interest in this investigation since it depicts the situation wherein an MTL mounted on a projectile would impact the earth at a large tilt angle and transmit back to the area from which it was launched.

In addition, since the theoretical calculations described in this study were made, the patterns of several MTL configurations superior to those in Section V as well as the quarter wave monopole over four quarter wave radial arms have been investigated experimentally. These measurements indicate an even greater superiority of the MTL over the quarter wave monopole for the geometry of particular interest described above. This is most likely due to the fact that when $\theta_t = 60°$ the radials do not shield the monopole from the earth and the theoretical calculations can be expected to be in error. Apparently this error tends to cause a theoretical prediction in field intensity greater than that which is observed in practice for the monopole. Since in a communication system the important factor is the minimum assured power level, and our measurements showed this minimum level to be several dB better for the MTL than for the monopole, we conclude that the MTL has better radiation characteristics for the application of primary interest in this work. An area of future work would be to determine better MTL configurations.

APPENDIX I

In this appendix two computer programs will be described. They are DIPOLE and WERFC and form the basis for all pattern calculations made in this report.

Figure 34 is a listing of subroutine DIPOLE. Included is a brief description of the program and definitions for the 12 input and 3 output parameters. Of these EXCIT, EX, EY, and EZ are complex, and the remainder are real. The program is an extension of equations developed by Norton[10] to include electric current elements of arbitrary position with respect to a fixed coordinate system. In Fig. 35 is shown an arbitrarily orientated electric current element located at the rectangular coordinates (XS, YS, ZS) meters. The xy plane is assumed to separate a lossy half-space, described by a relative dielectric constant ER and a conductivity SEMU expressed in emu (1 mho/meter = 10^{-11} emu), from air or free space. The lossy half-space is located at $z < 0$. The source is assumed to have an $e^{-j\omega t}$ time dependence with frequency FKC in kilohertz. It is desired to evaluate the field at a point described by the cylindrical coordinates (RF, PF, ZF) with RF and ZF expressed in meters and PF in radians. The orientation of the current element is described by THETA and PHI in radians as shown in Fig. 36. Here the x'y'z' rectangular coordinate system is the xyz system of Fig. 35 translated to the source point (XS, YS, ZS). The subroutine returns EX, EY, and EZ which are the x, y, and z components respectively of the electric field in volts/meter. NBUG enters the subroutine through a COMMON statement and is used in debugging. If NBUG = 1 the messages "ENTER DIPOLE" and "EXIT DIPOLE" will be printed when the subroutine is entered or exited respectively.

DIPOLE may be used only when the source point and the field point are in the air half-space, and are separated by at least a few free space wavelengths. The program has one difficulty. Errors sometimes occur when calculating the fields very near (less than one degree) the vertical axis. This difficulty can be overcome by interpolating the fields at either side of the vertical axis to obtain the fields at the vertical axis. In the far-field, the fields are varying slowly and interpolation may be done with high accuracy.

DIPOLE uses the complex function subprogram WERFC in evaluating the ground wave attenuation functions of Eqs. (9c) and (15b). Figure 37 is a listing of WERFC. Specifically

$$\text{WERFC}(z) = e^{-z^2}\,\text{erfc}(-jz), \qquad z = x+jy. \tag{39}$$

```
      SUBROUTINEDIPOLE(XS,YS,ZS,RF,PF,ZF,ER,SEMU,FKC,EXCIT,THETA,PHI,EX,
     2EY,EZ)
C*****************************************************************
C*****************************************************************
C     SUBROUTINE DIPOLE EVALUATES THE RECTANGULAR COMPONENTS OF THE
C     ELECTRIC FIELD OF A INFINITESIMAL ELECTRIC CURRENT LOCATED IN AIR
C     AND NEAR A LOSSY HALF - SPACE.  THE EQUATIONS USED ARE VALID when
C     THE FIELD POINT IS MORE THAN A FEW WAVELENGTHS FROM THE SOURCE.
C     REFERENCE FOR EQUATIONS IS 'THE PROPAGATION OF RADIO WAVES OVER
C     THE SURFACE OF THE EARTH AND IN THE UPPER ATMOSPHERE' BY K. A.
C     NORTON,  PROCEEDINGS OF THE IRE, VOL. 25, NUMBER 9, PAGE 1203.
C     INPUT PARAMETERS...
C     XS = X COORDINATE OF THE CURRENT ELEMENT IN METERS.
C     YS = Y COORDINATE OF THE CURRENT ELEMENT IN METERS.
C     ZS = Z COORDINATE OF THE CURRENT ELEMENT IN METERS.
C     RF = POLAR RADIUS OF THE FIELD POINT IN METERS.
C     PF = POLAR ANGULAR COORDINATE PHI OF THE FIELD POINT IN RADIANS.
C     ZF = Z COORDINATE OF THE FIELD POINT IN METERS.
C     ER = RELATIVE DIELECTRIC CONSTANT OF THE GROUND.
C     SEMU = CONDUCTIVITY OF THE GROUND IN EMU.  1 MHO/METER = 10**-11 EMU.
C     FKC = FREQUENCY IN KILOCYCLES.
C     EXCIT = COMPLEX MAGNITUDE OF THE CURRENT ELEMENT.
C     THETA = SPHERICAL THETA COORDINATE DESCRIBING CURRENT ELEMENT
C             ORIENTATION IN RADIANS.
C     I      SPHERICAL PHI COORDINATE DESCRIBING CURRENT ELEMENT
C             ORIENTATION IN RADIANS.
C     OUTPUT PARAMETERS...
C     EX = X COMPONENT OF THE ELECTRIC FIELD IN VOLTS/METER.
C     EY = Y COMPONENT OF THE ELECTRIC FIELD IN VOLTS/METER.
C     EZ = Z COMPONENT OF THE ELECTRIC FIELD IN VOLTS/METER.
C     NOTE  NBUG ENTERS THE SUBROUTINE THROUGH COMMON.  IF NBUG = 1 THE
C     MESSAGES 'ENTER DIPOLE' AND 'EXIT DIPOLE' ARE PRINTED WHEN THE
C     SUBROUTINE IS ENTERED OR EXITED RESPECTIVELY.
C     SUBROUTINE WERFC IS USED.
C*****************************************************************
C*****************************************************************
      COMPLEXEX1,EX2,E1,E2,X1,X2,X3,Q1,V,G,EXCIT
      COMPLEXXK2,XJ,U,PP,WP,RV,F,P1,W,  RH,EZV,ERV,EPV,EZH,ERH,EPH,EX,
     2EY,EZ
      COMPLEXIX,IY,IZ,RE,EP,ERPH,EPPH,EZPH
      COMPLEXWERFC
      COMMONNBUG
      IF(NBUG.EQ.1)WRITE(6,1)
    1 FORMAT(5X,'ENTER DIPOLE')
      XJ=CMPLX(0.0,1.0)
      PI=4.0*ATAN(1.0)
      A=ZS
      C=2.998E8
      WAVE=C/(FKC*1000.0)
      XK  =2.0*PI/WAVE
C
C     SET UP COORDINATES.
C
      XPF=RF*COS(PF)-XS
      YPF=RF*SIN(PF)-YS
      ZPF=ZF
      RPF=SQRT(XPF*XPF+YPF*YPF)
      PPF=ATAN2(YPF,XPF)
      R=SQRT(RPF*RPF+ZPF*ZPF)
      XX=1.8E18*SEMU/FKC
      XK2=CSQRT(ER+XJ*XX)*XK
      U=XK/XK2
```

Fig. 34. Computer listing of subroutine DIPOLE.

```
      R2=SQRT(RPF**RPF+(ZPF+A)**(ZPF+A))
      R1=SQRT(RPF**RPF+(ZPF-A)**(ZPF-A))
      SNCP=ZPF/R
      SNCPP=(ZPF+A)/R2
      PP=XJ*XK*R2*U-U/2.0
      WP=PP**(1.0+(A+ZPF)/(U*R2))**2
      CSCP=SQRT(1.0-SNCP**SNCP)
      RV=U*CSQRT(1.0-(U*CSCP)**(U*CSCP))
      RV=(SNCP-RV)/(SNCP+RV)
      B=ATAN((RP+CSCP*CSCP)/XX)
      P=PI*R2*COS(B)/(AA*WAVE)
      P1=P*CEXP(XJ*B)
      W=4.0*P1/((1.0-RV)**(1.0-RV))
      F=1.0+XJ*CSQRT(PI*W)*WERFC(CSQRT(W))
      SNCPP=(ZPF-A)/R1
      CSCPP=SQRT(1.0-SNCPP**2)
      EX1=XJ*XK*R1
      EX2=XJ* K*R2
      E1=CEXP(EX1)/R1
      E2=CEXP(EX2)/R2
      X1=(1.0/EX1)-(1.0/EX1**2)
      X2=(1.0/EX2)-(1.0/EX2**2)
      X3=CSQRT(1.0-U**2*CSCP**2)
C
C     DETERMINE EZV
C
      EZV=CSCPP**2*E1+RV*CSCP**2*E2
      EZV=EZV+(1.0-RV)*(1.0-U*U+U**4*CSCP**2)*F*E2
      EZV=EZV-U*X3*(2.0*SNCP)*E2/EX2
      EZV=EZV-E1*X1*(1.0-3.0*SNCPP)
      EZV=EZV-E2*X2*(1.0-3.0*SNCP)
      EZV=XJ*XK*EZV
      A1=CABS(EZV*R/(2.0*XK))
C
C     DETERMINE ERV
C
      ERV=SNCPP*CSCPP*E1+RV*SNCP*CSCP*E2
      ERV=ERV-CSCP*(1.0-RV)*U*X3*F*E2*(1.0-0.5*U**2*X3**2+0.5*SNCP**2-0.
     25/EX2)
      ERV=ERV+SNCP*CSCP*(1.0-RV)*E2/EX2
      ERV=ERV-3.0*SNCPP*CSCPP*X1*E1+CSCP*U*X3*(1.0-RV)*E2/(2.0*EX2)-3.0*
     2SNCP*CSCP*X2*E2
      ERV=-XJ*XK*ERV
C
C     DETERMINE EPV.
C
      EPV=CMPLX(0.0,0.0)
      RH=(X3-U*SNCP)/(X3+U*SNCP)
      BP=ATAN((ER-CSCP**2)/XX)
      Q=PI*XX*R2/(COS(BP)*WAVE)
      Q1=-Q*CEXP(-XJ*BP)
      V=4.0*Q1/(1.0+RH)**2
      G=1.0+XJ*CSQRT(PI*V)*WERFC(CSQRT(V))
C
C     DETERMINE EZH.
C
      EZH=SNCPP*CSCPP*E1-RV*SNCP*CSCP*E2+CSCP*(1.0-RV)*U*X3*F*E2*(1.0-
     2U*U+0.5*X3**2+0.5*SNCP**2-0.5/EX2)
      EZH=EZH-SNCP*CSCP*(1.0-RV)*E2/EX2-3.0*SNCPP*CSCPP*X1*E1
      EZH=EZH-CSCP*(1.0-RV)*U*X3*E2/(2.0*EX2)+3.0*SNCP*CSCP*X2*E2
      EZPH=XJ*XK*EZH
      EZH=EZPH*COS(PPF)
```

Fig. 34.

```
C
C      DETERMINE ERH.
C
       ERH=SNCPP**2*E1-RV*SNCP**2*E2+(1.0+RH)*G*E2-CSCP**2*U**2*(1.0-RV)
      2*F*E2
       ERH=ERH-X1*(1.0-3.0*CSCPP**2)*E1+X2*(1.0-3.0*CSCP**2)*(1.0-U**2*
      2(1.0+RV)-U**2*(1.0-RV)*F)*E2
       ERH=ERH+U**2*CSCP**2*(1.0-RV)*(1.0-1.0/EX2)*(F*(U**2*X3-SNCP**2
      3-1.0/EX2)+1.0/EX2)*E2
       ERPH=-XJ*XK*ERH
       ERH=ERPH*COS(PPF)
C
C      DETERMINE EPH.
C
       EPH=E1-RH*E2+(1.0+RH)*G*E2-(1.0-1.0/EX1)*E1/EX1
       EPH=EPH+(1.0-1.0/EX2)*(1.0-U**2*(1.0+RV)-U**2*(1.0-RV)*F)*E2/EX2
       EPH=(EPH+0.5*U**2*(1.0-RV)*(F*(U**2*X3-SNCP**2-1.0/EX2)+1.0/EX2)*
      2E2/EX2
       EPPH=XJ*XK*EPH
       EPH=EPPH*SIN(PPF)
C
C      PLACE PROPER MAGNITUDE AND PHASE ON ALL COMPONENTS.
C
C
C      CONVERT TO RECTANGULAR COORDINATES.
C
       IX=EXCIT*SIN(THETA)*COS(PHI)
       IY=EXCIT*SIN(THETA)*SIN(PHI)
       IZ=EXCIT*COS(THETA)
       RE=IX*ERH+IY*ERPH*SIN(PPF)+IZ*ERV
       EP=IX*EPH-IY*EPPH*COS(PPF)
       EZ=IX*EZH+IY*EZPH*SIN(PPF)+IZ*EZV
       EX=RE*COS(PPF)-EP*SIN(PPF)
       EY=RE*SIN(PPF)+EP*COS(PPF)
       IF(NBUG.EQ.1)WRITE(6,2)
 2     FORMAT(20X,'EXIT DIPOLE')
       RETURN
       END
```

Fig. 34.

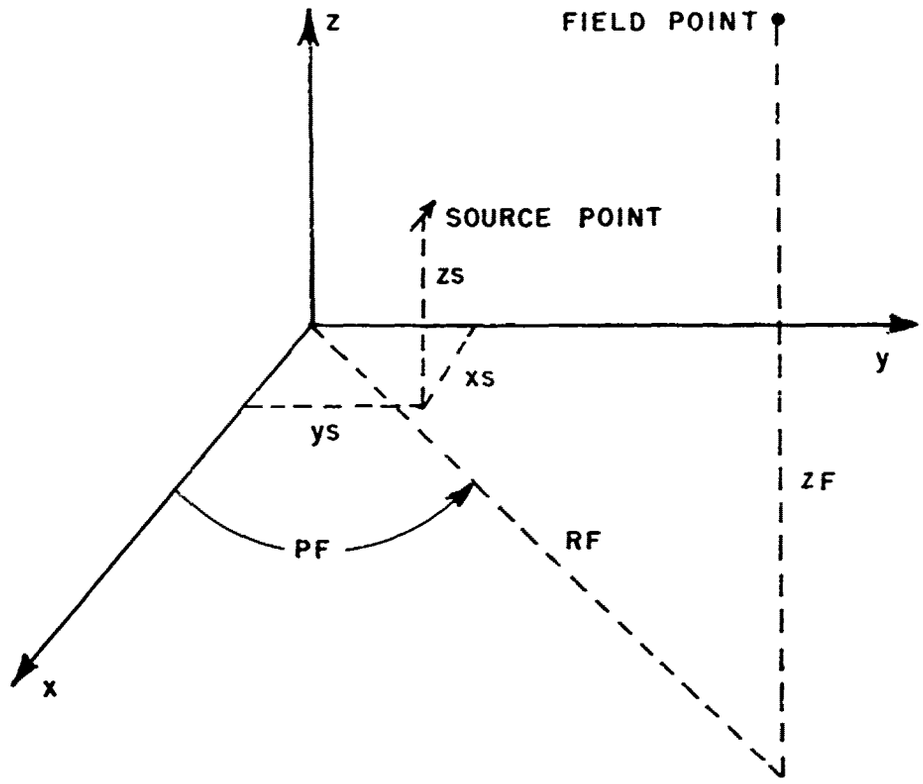

Fig. 35. Location of the source in subroutine DIPOLE.

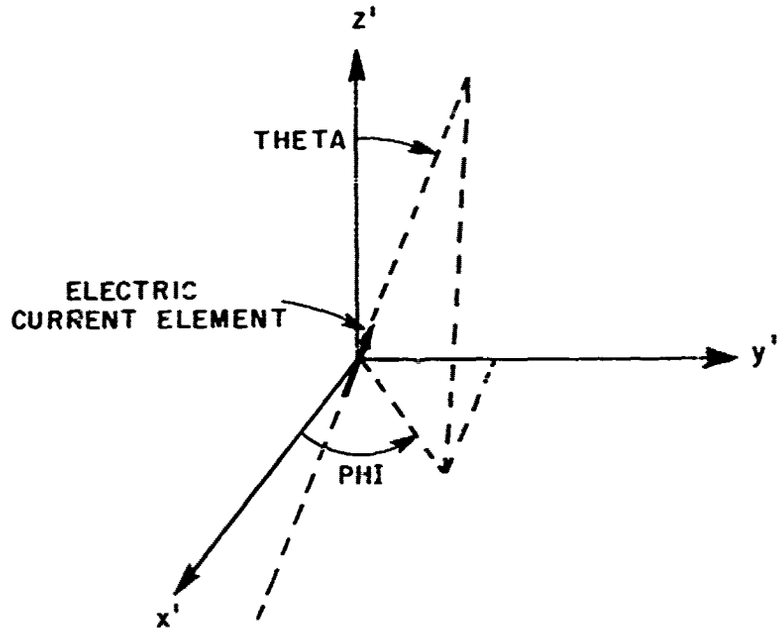

Fig. 36. Orientation of the source in subroutine DIPOLE.

```
      COMPLEXFUNCTIONWERFC(Z)
C
C     WERFC(Z) EVALUATES W(Z) = EXP(-Z**2)*ERFC(-J*Z) USING N.B.S.
C     EQS. 7.1.23 AND 7.1.29.
C
      COMPLEXWERFC,Z,XJ,ZZ,ERFC,A,B,C
      COMMONNBUG
      COSH(X)=(EXP(X)+EXP(-X))/2.0
      SINH(X)=(EXP(X)-EXP(-X))/2.0
      F(X,Y,N)=2.0*X-2.0*X*COSH(N*Y)*COS(2.0*X*Y)+N*SINH(N*Y)*SIN(2.0*X*
     2Y)
      G(X,Y,N)=2.0*X*COSH(N*Y)*SIN(2.0*X*Y)+N*SINH(N*Y)*COS(2.0*X*Y)
      IF(NBUG.EQ.1)WRITE(6,1)
    1 FORMAT(5X,'ENTER WERFC')
      PI=4.0*ATAN(1.0)
      XJ=CMPLX(0.0,1.0)
      ZZ=-XJ*Z
      X=REAL(ZZ)
      Y=AIMAG(ZZ)
C     WRITE(6,90)X,Y
      IF(ABS(X).GT.3.9.OR.ABS(Y).GT.3.0)GOTO200
      T=1.0/(1.0+.3275911*X)
      ERFX=1.0-(.254829592*T-.284496736*T**2+1.421413741*T**3-1.45315202
     27*T**4+1.061405429*T**5)*EXP(-X*X)
      C=ERFX*(EXP(-X*X)/(2.0*PI*X))*((1.0-COS(2.0*X*Y))+XJ*SIN(2.0*X*Y))
      A=CMPLX(0.0,0.0)
      I=0
      DO100N=1,100
      B=(EXP(-.25*N*N)/(N*N+4.0*X*X))*(F(X,Y,N)+XJ*G(X,Y,N))
      A=A+B
C     WRITE(6,90)A,B
   90 FORMAT(5X,4E15.5)
      IF(N.LE.2)GOTO100
      R1=ABS(REAL(B))
      R2=ABS(REAL(A))
      S1=ABS(AIMAG(B))
      S2=ABS(AIMAG(A))
      IF(R1/(R1+R2).LT.3.0E-6.AND.S1/(S1+S2).LT.3.0E-6)GOTO110
      I=0
      GOTO100
  110 I=I+1
      IF(I.GE.3)GOTO120
  100 CONTINUE
      WRITE(6,130)
  130 FORMAT(//5X,'ERFC FAILED TO CONVERGE',//)
  120 A=2.0*EXP(-X*X)*A/PI
      ERFC=1.0-(A+C)
      WERFC=ERFC*CEXP(-Z*Z)
```

Fig. 37. Computer listing of function subroutine WERFC.

```
      GOTO300
  200 ERFC=CMPLX(1.0,0.0)
      I=0
      NMAX=CABS(ZZ)
      NUM=1
      DO150N=1,NMAX
      NUM=-NUM*(2*N-1)
      A=ERFC
      ERFC=ERFC+NUM/(2.0*ZZ*ZZ)**N
      IF(N.LE.1)GOTO150
      XA=CABS(A)
      XE=CABS(ERFC)
      RAT=ABS(XA-XE)/XE
      IF(RAT.LT.1.0E-5)GOTO160
      I=0
      GOTO150
  160 I=I+1
      IF(I.GE.2)GOTO170
  150 CONTINUE
      IF(RA. .T.1.0E-3)WRITE(6,180)RAT
  180 FORMA     ,'WERFC FAILED TO CONVERGE     RATIO = ',E13.4/)
  170 WERFC  =  (Z*SQRT(PI))
  300 CONTI
      IF(NBUG    .1)WRITE(6,190)Z,WERFC
  190 FORMAT(5A,'Z = ',2E15.5,5X,'WERFC(Z) = ',2E15.6)
      IF(NBUG.EQ.1)WRITE(6,2)
    2 FORMAT(20X,'EXIT WERFC')
      RETURN
      END
```

Fig. 37.

The following formulae are used[11],

$$(40) \qquad \sqrt{\pi}\, z\, e^{z^2} \operatorname{erfc}(z) \sim 1 + \sum_{m=1}^{\infty} (-1)^m \frac{1\cdot 3\cdots(2m-1)}{(2z^2)^m}$$

for $|x| > 3.9$ or $|y| > 3.0$, and

$$(41) \qquad \operatorname{erf}(x+iy) = \operatorname{erf}(x) + \frac{e^{-x^2}}{2\pi x}[(1-\cos(2xy)) \div j\sin(2xy)]$$

$$+ \frac{2}{\pi} e^{-x^2} \sum_{n=1} \frac{e^{-n^2/4}}{n^2+4x^2}[f_n(x,y) + jg_n(x,y)]$$

otherwise. In Eq. (41)

$$(42a) \qquad \operatorname{erfc}(z) = \operatorname{erfc}(x+iy) = 1-\operatorname{erf}(z)$$

$$(42b) \qquad f_n(x,y) = 2x-2x\cosh(ny)\cos(2xy)+n\sinh(ny)\sin(2xy)$$

$$(42c) \qquad g_n(x,y) = 2x\cosh(ny)\sin(2xy)+n\sinh(ny)\cos(2xy).$$

NBUG enters this function subprogram through a COMMON statement and is used in debugging. If NBUG = 1 the messages "ENTER WERFC" and "EXIT WERFC" will be printed when the function subprogram is entered or exited respectively. Z and WERFC(Z) will also be printed if NBUG=1.

APPENDIX II

In this appendix far field-patterns, evaluated using subroutine DIPOLE described in Appendix I and approximations described in Sections II and IV, will be compared with patterns from the literature. In Figs. 38-40 we compare far-field patterns of infinitesimal electric current elements calculated using subroutine DIPOLE with patterns presented by Jordon and Balmain[14]. The ground parameters and frequency for these patterns are identified by the parameter n and by ε_r as follows:

$$n = \chi/\varepsilon_r \tag{43}$$

where

$$\chi = \frac{18 \times 10^3 \, \sigma_{\text{mho/meter}}}{f \text{ MHz}} \tag{44}$$

Each figure shows curves for n=1 and n=100, and the curves are normalized so that the n=100 curves have maximum field strength of 1.0. Figures 38-40 are for a vertical element at the earth's surface, a vertical element $\lambda/2$ above the earth, and a horizontal element $\lambda/2$ above the earth with the pattern in the yz plane (see Fig. 4) respectively. In addition our calculations have been found to have the proper rotation symmetries.

Next we will investigate an extended source, namely a vertical half-wave dipole with its center height one wavelength above a lossy earth. The frequency is 20 MHz and field patterns are shown for the elevation plane (see Fig. 4). Assuming the antenna to be in free space we approximate the antenna current as being sinusoidal. Using the trapezoidal rule and the methods of Section IV the antenna was represented by 11 vertical infinitesimal electric current elements. The fields of these 11 infinitesimal dipoles were determined using subroutine DIPOLE and then summed to yield the patterns shown in Fig. 41. Patterns calculated by Horn[15] are also shown. Fig. 41a is for σ = 0.1 mho/meter and ε_r = 30, and Fig. 41b is for σ = 0.01 mho/meter and ε_r = 10. Our patterns and those of Horn have been normalized so that the peak field strength of the patterns shown in Fig. 41a are unity. Note the excellent agreement of the location and magnitude of maximums and nulls in Fig. 41.

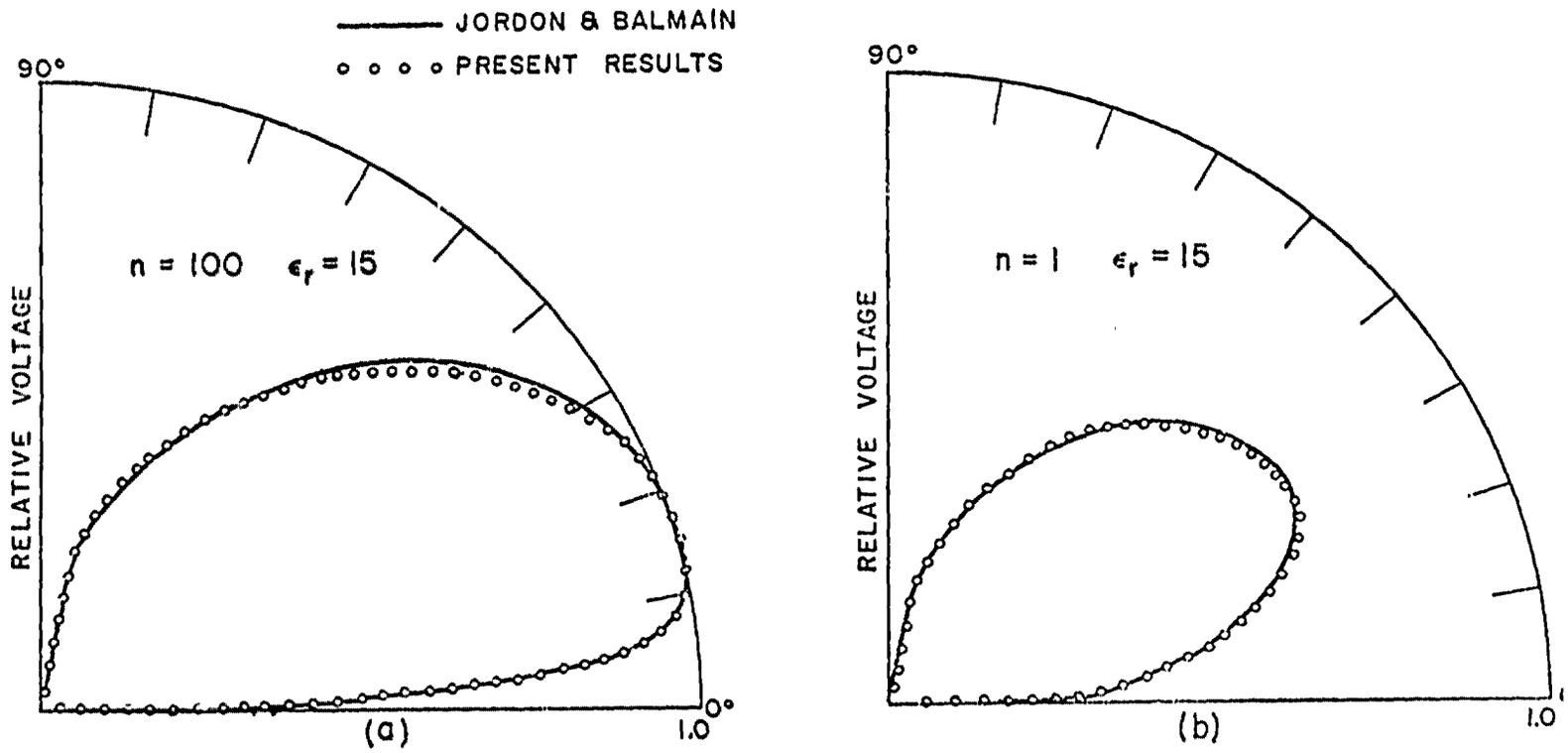

Fig. 38. Field pattern for a vertical element located at the surface of a lossy earth. (a) n=100, (b) n=1.

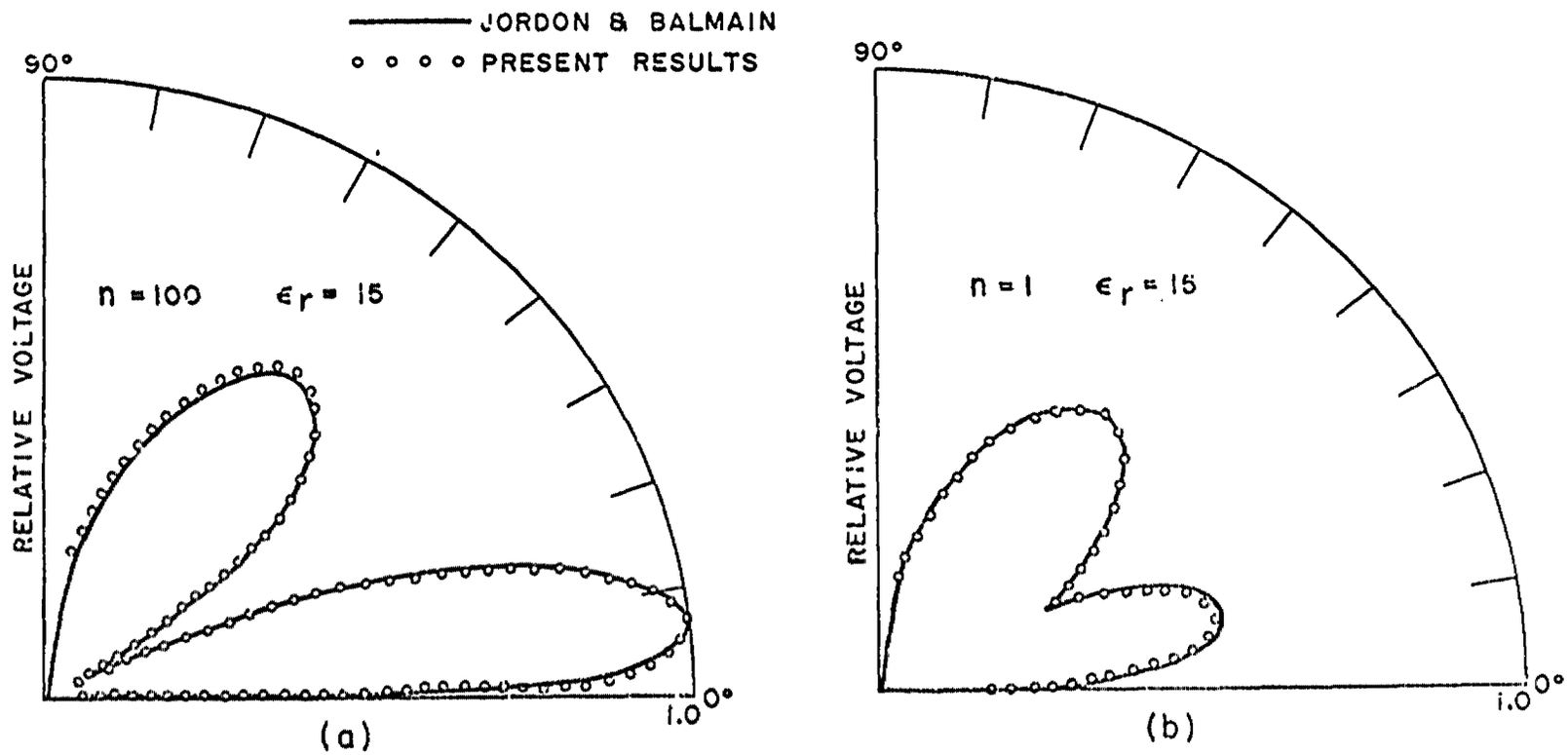

Fig. 39. Field pattern for a vertical element located $\lambda/2$ above a lossy earth. (a) n=100, (b) n=1.

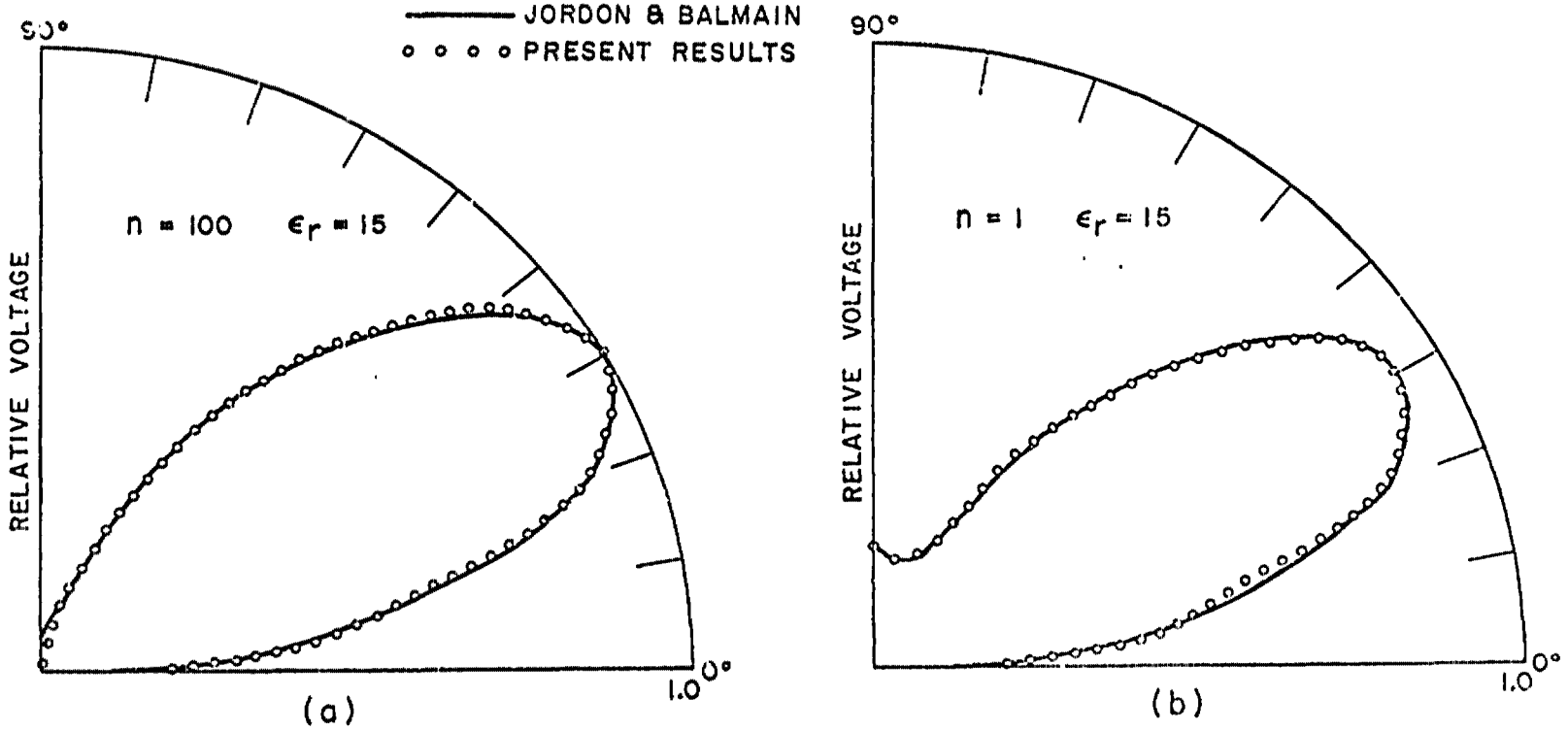

Fig. 40. Field pattern for a horizontal element located λ/2 above a lossy earth. Pactern in the plane perpendicular to the element axis. (a) n=1, (b) n=1.

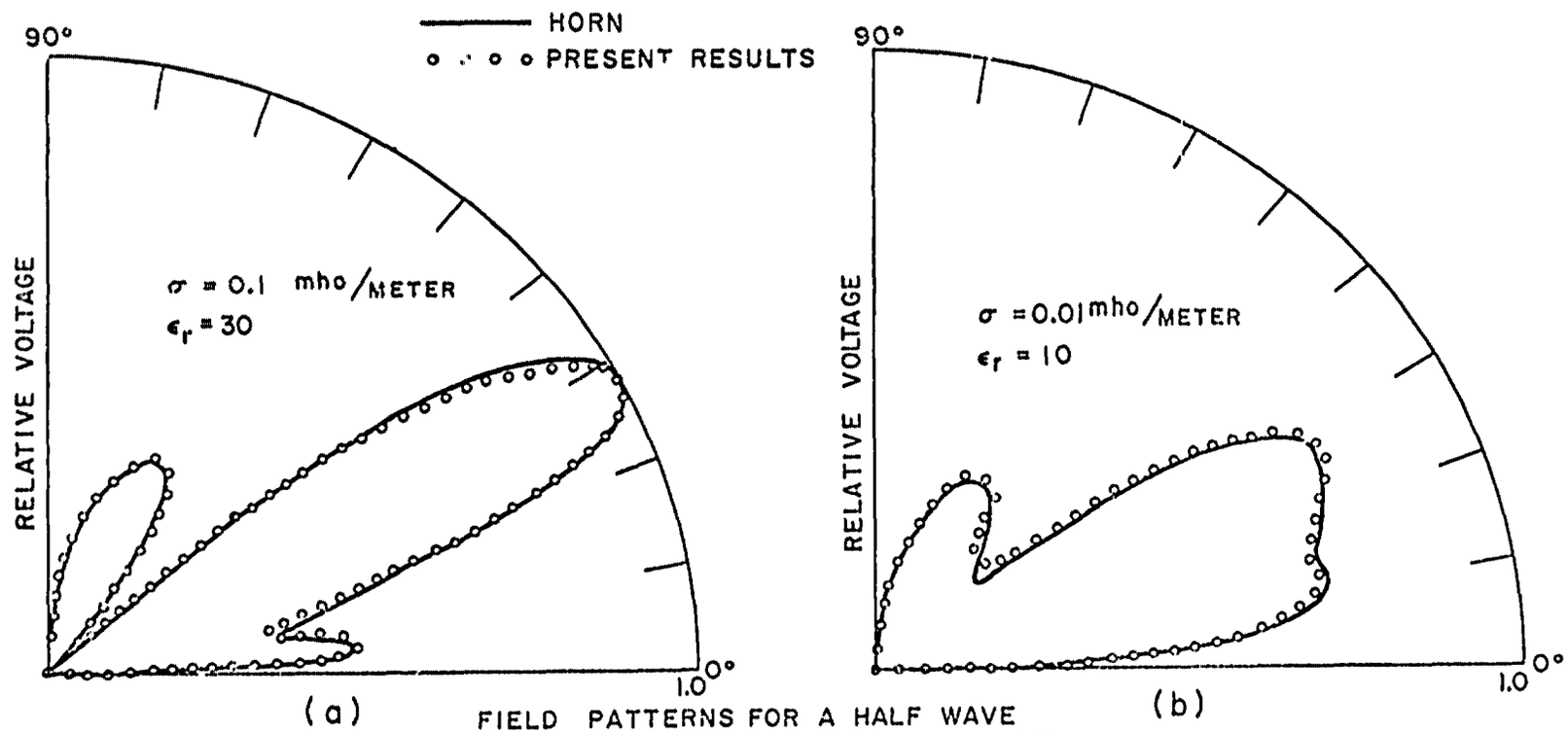

Fig. 41. Field pattern for a half wave vertical dipole with center height λ from a lossy earth.
(a) σ=0.1 mho/meter, ε_r=30.
(b) σ=0.01 mho/meter, ε_r=10.

REFERENCES

1. Sommerfeld, A., "Uber der Ausbreitung der Willen in der Drahtlosen Telegraphic," Ann. Physik., Vol. 28, (1909), pp. 663-737.

2. Sommerfeld, A., Partial Differential Equations in Physics, Academic Press, (1964), New York.

3. Banos, A., Dipole Radiation in the Presence of a Conducting Half-Space, Pergamon Press, (1966), New York.

4. Miller, E.K., Poggio, A.J., Burke, G.J., and Selden, E.K., "Analysis of Wire Antennas in the Presence of a Conducting Half-Space: Part I. The Vertical Antenna in Free Space," Canadian Journal of Physics, Vol. 50, No. 9, May 1, 1972.

5. Miller, E.K., Poggio, A.J., Burke, G.J., and Selden, E.K., "Analysis of Wire Antennas in the Presence of a Conducting Half-Space: Part II. The Horizontal Antenna in Free Space," Canadian Journal of Physics, (to be published).

6. Richmond, J.H., "Computer Analysis of Three Dimensional Wire Antennas," Report 2708-4, 22 December 1969, ElectroScience Laboratory, Department of Electrical Engineering, The Ohio State University; prepared under Contract DAAD05-69-C-0031 for the Ballistic Research Laboratory, Department of the Army, Maryland.

7. Thiele, G.A., "Wire Antennas," Ch. 2 in Numerical Techniques for Electromagnetic Boundary Value Problems, Prof. R. Mittra, Editor, Pergamon Press, London (to be published).

8. Agrawal, P.K., "Numerical Solution of Wire Antennas in a Cavity," PhD. Dissertation, (1972), The Ohio State University.

9. Chao, H.H. and Strait, B.J., "Computer Programs for Radiation and Scattering by Arbitrary Configurations of Bent Wires," Scientific Report No. 7, 15 September 1970, Electrical Engineering Department, Syracuse University; prepared under Contract F19628-68-C-0180 for Air Force Cambridge Research Laboratories Air Force Systems Command, Bedford, Massachusetts.

10. Norton, K.A., "The Propagation of Radio Waves Over the Surface of the Earth and in the Upper Atmosphere. Part II. The Propagation from Vertical, Horizontal, and Loop Antennas Over a Plane Earth of Finite Conductivity," Proceeding of the Institute of Radio Engineers, Vol. 25, No. 9, Sept. (1937), pp. 1203-1236.

11. Handbook of Mathematical Functions, U. S. Department of Commerce, National Bureau of Standards, Applied Mathematical Series - 55, Chapter 7.

12. Bohley, P., Private Communication.

13. Wheeler, H.A., "The Radiansphere Around a Small Antenna," Proceedings of the Institute of Radio Engineers, Vol. 47, No. 8 August (1959), pp. 1325-1331.

14. Jordon, E.C. and Balmain, K.G., Electromagnetic Waves and Radiating Systems, Prentice-Hall, Inc., Englewood Cliffs, New Jersey, (1968), Chapter 16.

15. Horn, J.M., "HF Vertical-Plane Patterns of Monopoles and Elevated Vertical Dipoles With and Without Extended Ground Systems," Naval Electronics Laboratory Center Report 1567, June 1968, San Diego, California.